NOAA Technical Memorandum NMFS-AFSC-428

Geographically Stratified Abundance Estimate for Bering-Chukchi-Beaufort Seas Bowhead Whales (*Balaena mysticetus*) from an August 2019 Aerial Line-Transect Survey in the Beaufort Sea and Amundsen Gulf

M. C. Ferguson, J. T. Clarke, A. L. Willoughby, A. A. Brower, and A. D. Rotrock

November 2021

U.S. DEPARTMENT OF COMMERCE

National Oceanic and Atmospheric Administration
National Marine Fisheries Service
Alaska Fisheries Science Center

The National Marine Fisheries Service's Alaska Fisheries Science Center uses the NOAA Technical Memorandum series to issue informal scientific and technical publications when complete formal review and editorial processing are not appropriate or feasible. Documents within this series reflect sound professional work and may be referenced in the formal scientific and technical literature.

The NMFS-AFSC Technical Memorandum series of the Alaska Fisheries Science Center continues the NMFS-F/NWC series established in 1970 by the Northwest Fisheries Center. The NMFS-NWFSC series is currently used by the Northwest Fisheries Science Center.

This document should be cited as follows:

Ferguson, M.C., J. T. Clarke, A. L. Willoughby, A. A. Brower, and A. D. Rotrock. 2021. Geographically stratified abundance estimate for Bering-Chukchi-Beaufort Seas bowhead whales (*Balaena mysticetus*) from an August 2019 aerial line-transect survey in the Beaufort Sea and Amundsen Gulf. U.S. Dep. Commer., NOAA Tech. Memo. NMFS-AFSC-428, 56 p

This document is available online at:

Document available: https://repository.library.noaa.gov

NOAA FISHERIES

Geographically Stratified Abundance Estimate for Bering-Chukchi-Beaufort Seas Bowhead Whales (*Balaena mysticetus*) from an August 2019 Aerial Line-Transect Survey in the Beaufort

M. C. Ferguson[1,2], J. T. Clarke[1,3], A. L. Willoughby[1,3], A. A. Brower[1,3], and A. D. Rotrock[1,3]

[1]Marine Mammal Laboratory
Alaska Fisheries Science Center
National Marine Fisheries Service
National Oceanic and Atmospheric Administration
7600 Sand Point Way NE
Seattle, WA 98115

[3]Cooperative Institute for Climate, Ocean, and Ecosystem Studies
University of Washington
John M. Wallace Hall
3737 Brooklyn Ave NE
Seattle, WA 98105

[2]School of Aquatic and Fishery Sciences
University of Washington
1122 NE Boat St
Seattle, WA 98195-5020

U.S. DEPARTMENT OF COMMERCE

National Oceanic and Atmospheric Administration
National Marine Fisheries Service
Alaska Fisheries Science Center

NOAA Techncial Memorandum NOAA-TM-AFSC-428

November 2021

ABSTRACT

To derive a new estimate of abundance for the Bering-Chukchi-Beaufort Seas population of bowhead whales, we conducted aerial line-transect surveys over the whales' summer range in the Beaufort Sea shelf and Amundsen Gulf during August 2019. A geographically stratified analysis, incorporating correction factors for transect detection probability and availability bias, was used to estimate bowhead whale abundance in three regions. The regional abundance estimate for Amundsen Gulf was 275 whales (CV = 0.550; bootstrap 95% CI [83, 654]), the eastern Beaufort Sea was 13,207 whales (CV = 0.570; bootstrap 95% CI [7,108, 27,522]), and the western Beaufort Sea was 1,049 whales (CV = 0.538; bootstrap 95% CI [252, 2,132]), resulting in an estimated total abundance of 14,531 whales (CV = 0.540; bootstrap 95% CI [7,968, 29,376]). A bootstrap sensitivity analysis suggested that the largest contributors to the uncertainty in the overall abundance estimate were the transect detection probability and variability among the line-transect survey sample units.

CONTENTS

INTRODUCTION

The Bering-Chukchi-Beaufort Seas (BCB) population of bowhead whales (*Balaena mysticetus*) is listed as Endangered under the U.S. Endangered Species Act and it is an important nutritional, spiritual, and cultural resource for Alaska Natives (Braund and Associates 2018). This population's range encompasses the Bering, Chukchi, and Beaufort seas (Moore and Reeves 1993). These bowhead whales can live longer than 200 years (George et al. 1999, 2021). To effectively conserve and manage this long-lived species in a time of unprecedented environmental change, estimates of population abundance and trends, and associated uncertainty, are critical.

Reliable population abundance estimates for BCB bowhead whales date back to 1978 when ice-based visual and acoustic surveys were first conducted as the whales rounded Point Barrow, Alaska, during their spring migration (Krogman et al. 1989). Between 1978 and 2011, there were 21 attempted ice-based surveys (George et al. 2013) which resulted in a series of 12 abundance estimates (Muto et al. 2020) that are considered the gold standard for BCB bowhead whales (Suydam et al. 2019). There were also three abundance estimates (1986, 2004, and 2011) derived from aerial imagery using photo identification in a mark-recapture framework (da Silva et al. 2000, Koski et al. 2010, Givens et al. 2018). Prior to 2019, the most recent population abundance estimates were for 2011, when both an ice-based visual survey and an aerial photo-identification survey were conducted during spring, resulting in estimates of 16,820 (CV = 0.052; Givens et al. 2016) and 27,133 (CV = 0.217; Givens et al. 2018) whales,

respectively. Based on the ice-based surveys, Givens et al. (2016) estimated the annual rate of increase from 1978 (4,765 whales) to 2011 to be 3.7% (95% CI = 2.9-4.6%).

During 2019, a spring ice-based visual survey and a summer aerial line-transect survey were conducted with the goal of generating independent abundance estimates for BCB bowhead whales during the same year. The estimated abundance from the 2019 ice-based survey was 14,025 whales (CV = 0.228; Givens et al. 2020, 2021). The results of the 2019 aerial survey and geographically stratified abundance estimate are reported here.

This paper has four objectives:

- Provide an overview of the 2019 aerial line-transect survey methods and results.
- Derive an estimate of the population abundance of BCB bowhead whales from line-transect aerial survey data collected in the Beaufort Sea and Amundsen Gulf during August 2019 using geographically stratified analytical methods.
- Estimate the uncertainty in the BCB bowhead whale abundance estimate.
- Evaluate the contribution of each component of the analysis to the uncertainty in the abundance estimate to determine how field and analytical methods may be improved to reduce uncertainty.

METHODS

Data Collection

Brief overviews of the field methods and imagery analysis protocols are provided here. See Clarke et al. (2019), Clarke et al. (2020), and ASAMM (2019) for detailed field methods and Willoughby et al. (2021) for detailed imagery collection and analysis methods.

Aerial Line-transect Surveys

The 2019 aerial line-transect surveys were conducted in August, covering most of the summer range of BCB bowhead whales, encompassing the Beaufort Sea shelf and a portion of Amundsen Gulf (Fig. 1; total area 203,885 km^2). These surveys were conducted by the Aerial Surveys of Arctic Marine Mammals (ASAMM) project, and were funded and co-managed by the U.S. Bureau of Ocean Energy Management (BOEM) and U.S. National Oceanic and Atmospheric Administration (NOAA). ASAMM was a long-term monitoring project that conducted aerial line-transect surveys for marine mammals in the eastern Chukchi or western Beaufort seas every summer or autumn from 1979 to 2019.

Systematic transects were placed 19 km apart, based on a grid with a randomly selected start point (Figure 1). Transects were oriented perpendicular to the coastline, from shore to the 200-m isobath. Some transects in the western Beaufort Sea extended to the 2,000-m isobath to determine whether the bowhead whale distribution extended beyond the shelf break. Three survey strata (regions) were defined based on expected bowhead whale densities: Amundsen Gulf (AG; light purple polygon in Fig. 1; total area 29,424 km^2), eastern Beaufort Sea (EBS; light

yellow polygon in Fig. 1; total area 120,614 km^2), and western Beaufort Sea (WBS; light green polygon in Fig. 1; total area 53,848 km^2).

One Turbo Commander aircraft (abbreviated cmdr in parameter subscripts) based in Deadhorse, Alaska, USA, surveyed the western Beaufort Sea. One Turbo Commander aircraft based in Inuvik, Northwest Territories, Canada, surveyed the eastern Beaufort Sea and Amundsen Gulf. The two Turbo Commanders had identical configurations, with the exception that the aircraft based in Inuvik had a belly port with a mounted camera. One De Havilland Twin Otter aircraft (abbreviated ott in parameter subscripts) surveyed the eastern Beaufort Sea and Amundsen Gulf. The Twin Otter was initially based in Ulukhaktok, Northwest Territories, Canada, but relocated to Inuvik when aviation fuel was no longer available for purchase in Ulukhaktok. Surveys were flown 305-460 m above ground level at a survey speed of 213 km/hr. All three aircraft had bubble windows for the left- and right-side primary observers. Bubble windows in the Twin Otter were smaller than those in the Turbo Commanders.

Each survey team comprised two primary observers and one dedicated data recorder. Twelve observers participated in the bowhead abundance surveys during August 2019. All observers were experienced field biologists and most (75%) had previous experience with ASAMM surveys, ensuring consistency in data collection across years. ASAMM field experience ranged from 1 to 25 years (median = 7.0 years). Less experienced ASAMM observers were integrated into teams consisting of more experienced ASAMM observers and all observers were provided feedback throughout the field season to help maintain data consistency.

The data recorder used custom-built, menu-driven software to enter sighting data into a laptop computer interfaced with a Global Position System (GPS). Time and position data

(latitude, longitude, altitude) were automatically recorded every 30 seconds (in time) or whenever a manual data entry was recorded. Environmental and viewing conditions, including integer-valued Beaufort Sea State, visibility range perpendicular to the aircraft on each side of the plane (<1 km, 1-2 km, 2-3 km, 3-5 km, 5-10 km, or unlimited), sky conditions (clear, partly cloudy, overcast), integer-valued sea ice percent on each side of the plane, and impediments to visibility (glare, fog, haze, precipitation, ice on the window, low ceiling) on each side of the plane were recorded every 5 minutes (in time) or whenever conditions changed. Primary observers scanned with naked eye, using binoculars only to check potential targets or get a magnified view on a confirmed target. Declination angles from the horizon to each sighting were measured using handheld Suunto clinometers when the sighting was abeam. One "sighting" was defined as all animals within 5 body lengths of each other. Once the clinometer angle was recorded, most sightings of large cetaceans (i.e., anything larger than a beluga, *Delphinapterus leucas*) were circled to confirm species identification, determine a final group size estimate, look for calves, and determine behavior. Both initial and final group size estimates were recorded in the database; if group size could not be determined with certainty, high or low estimates were recorded. Separate fields in the database distinguished between calves initially detected from the transect and calves that were only detected during circling. Circling did not commence in special circumstances, such as restrictions due to weather, fuel, time of day, or duty hours, or in the vicinity of subsistence hunting activities. Sightings that could not be positively identified to species were recorded at the taxonomic level to which they could be identified (e.g., unidentified cetacean). The observers watched for any abrupt and

unexpected changes in the whales' initial observed behavior and any observed responses were recorded in the database, along with the number of whales that responded.

Ten survey modes were defined for data collection (Clarke et al. 2020), although only six are relevant here: transect, circling from transect, Cetacean Aggregation Protocols (CAPs), CAPs circling, search, and circling from search. During all six of these survey modes, observers were actively surveying and all sightings and effort data were recorded. Transect effort refers to systematic survey effort along a prescribed transect line. Search refers to non-systematic survey effort during transit or between transects. Circling from search or transect occurred when the aircraft diverted from flat and level flight to circle a localized area to investigate a sighting or potential sightings. Standard line-transect survey protocols (Buckland et al. 2001) were followed until bowhead whale encounter rates exceeded the observers' ability to accurately record location and clinometer angle to each sighting. In these areas with extremely high densities of bowhead whales, CAPs were used, wherein the survey team flew through the high-density patch in passing mode to collect accurate encounter rate data, and then flew back through the patch in closing (CAPs circling) mode to collect information on group size, number of calves, and behavior. The CAPs are documented in Clarke et al. (2020).

Belly Port Imagery

During ASAMM surveys in 2018 and 2019, one Turbo Commander collected true color (red, green, and blue [RGB]) imagery from a Nikon-D810 digital SLR camera with a 20- or 21-mm lens mounted to a belly port. At 400 m survey altitude, a single image taken with the 21-mm lens captured a parcel of water measuring approximately 684 m perpendicular to the transect

(342 m on each side of the transect) and 457 m along the transect. Imagery was collected every 2 to 3 seconds, resulting in each parcel of water being visible in three to four images. Metadata automatically written to each image included latitude, longitude, date, and time. Every third image collected was manually reviewed post-flight for marine mammal sightings by trained photo analysts (Willoughby et al. 2021). Any sightings detected in the imagery were compared to the visual survey database to determine matches based on date, time, and location (side of plane and distance from transect).

Field-of-View Trials

To estimate the amount of time observers had to view objects as a function of perpendicular distance to the transect, in 2018 and 2019 field-of-view (FOV) trials were flown by each aircraft type over land using a fixed structure (a Conex box for the Turbo Commander and a cabin for the Twin Otter) as a target. See Clarke et al. (2020) for additional details about the FOV trial methods. An FOV trial is defined as one flight down a transect. Multiple trials (replicates) were flown at pre-determined transects located at 500 m and 2,000 m perpendicular distance from the target. These time-in-view estimates were incorporated into the availability bias correction factors.

Data Analyses

We derived a geographically stratified line-transect abundance estimate with corrections for transect detection probability (P_0) and availability bias (P_a). Uncertainty estimates and sensitivity analyses were conducted using a bootstrap algorithm that

incorporated both parametric and non-parametric sampling. Each component of the analysis is discussed below. All analyses were conducted in R version 3.6.2 (R Core Team 2019) with packages mrds (Laake et al. 2016), lme4 (Bates et al. 2015), sp (Pebesma and Bivand 2005; Bivand et al. 2013), rgdal (Bivand et al. 2019), rgeos (Bivand and Rundel 2019), and maptools (Bivand and Lewin-Koh 2019).

Detection Functions

The detection function models how an observer's ability to detect animals decreases with increasing distance from the transect and possibly other factors (Marques and Buckland 2003). Assuming animals are uniformly distributed within the strips searched on both sides of the transect, the distribution of perpendicular distances from the transect to sightings can be used to model the detection function, $g(y)$ (Buckland et al. 2001). Separate detection function models were built for the Twin Otter and the Turbo Commander due to differences in window design and aircraft configuration that likely affected detectability. This decision was based on expert judgment rather than a formal statistical test because the latter likely would be unreliable due to the extremely unbalanced sample sizes for the two types of aircraft.

The line-transect data were filtered prior to modeling the detection function. Only bowhead whale sightings made by primary observers during transect, CAPs, and search effort with recorded declination angles were used in the detection function analyses. All analyses were limited to data collected during conditions of Beaufort Sea State 5 or less. The detection function for the Twin Otter was based on data from only 2019, the single year in which this specific type of aircraft was used to fly ASAMM surveys. The exact same configuration of Turbo

Commander used during the August 2019 bowhead abundance surveys flew ASAMM surveys every year since 2009, so the complete time series (2009-2019) of Turbo Commander data was used to model its detection function (Fig. 2).

Sighting data were truncated very close to and far from the transect. Data were left-truncated to account for lower sighting probabilities very close to the aircraft (Hain et al. 1999). Based on visual inspection of histograms of perpendicular sighting distances for bowhead whales, the Twin Otter data were left-truncated at 350 m (Fig. 3) and the Turbo Commander data were left-truncated at 75 m (Fig. 4). The left-truncation (ltrnc) distance for each aircraft is referred to as $y_{ltrnc,aircraft}$, where aircraft designation is "o" for the Twin Otter and "c" for the Turbo Commander. Hereafter, reference to the transect implicitly means $y_{ltrnc,aircraft}$. The farthest 5% of sightings for each aircraft type were omitted from the detection function analyses to minimize the effects of outliers. The perpendicular distance of the farthest sighting remaining after right-truncation (rtrnc) is referred to as $y_{rtrnc,aircraft}$.

To account for variable visibility perpendicular to the transect due to impediments (e.g., precipitation, fog, and haze), sighting-specific search widths were used to model the detection function. We refer to these widths as $w_{v,i}$. The value of $w_{v,i}$ for each sighting was computed by converting the categorical variables for perpendicular visibility on the sighting's side of the aircraft into integer-valued distances as follows: "< 1 km" = 1 km, "1-2 km" = 2 km, "2-3 km" = 3 km, "3-5 km" = 5 km, "5-10 km" = 10 km, and "unlimited" = 20 km. Call this integer Vis_i. The smaller value of Vis_i or the right-truncation distance for the aircraft ($y_{rtrnc,aircraft}$) was assigned to $w_{v,i}$: $w_{v,i} = \min(Vis_i, y_{rtrnc,aircraft})$. The index v distinguishes among elements in the set of unique Vis values from 1 to $y_{rtrnc,aircraft}$. Detection functions for each aircraft type were generated using

multiple covariates distance sampling methods (Marques and Buckland 2003) for "single observer" (no mark-recapture) platforms using the ddf function in the R package mrds (Laake et al. 2016). The integration range for computing detection probability was specified via the int.range argument for ddf, with the number of rows corresponding to the number of observations and the width variable set to $w_{v,i}$. Detection function models, g(y,z), with hazard-rate and half-normal key functions, each with second-order cosine series adjustments, were considered. The null hazard-rate models had considerably lower AIC values and exhibited better fit than the half-normal models or models with cosine series adjustments, so forward stepwise selection of covariates, using AIC as the model selection criterion, proceeded with only the hazard-rate key function.

Covariates evaluated for inclusion in the detection function models are defined in Table 1. Depth and longitude variables were examined to accommodate potential differences in behavior, which might affect detectability, due to differences in habitat, habitat use, or anthropogenic disturbance across the study area. Detectability might depend on group size, so several group size covariates were considered. Beaufort Sea State affects an observer's ability to detect target species against the noise of whitecaps and waves, so two sea state variables were considered. Surveys were infrequently conducted when sea ice cover was greater than 10%; therefore, to provide balanced sample sizes, a categorical variable indicating only whether sea ice cover was < 10 % or ≥ 10 % was considered.

Surveys were infrequently conducted when sea ice cover was greater than 10%; therefore, to provide balanced sample sizes, a categorical variable indicating only whether sea ice cover was < 10 % or ≥ 10 % was considered. For instances in which there were multiple

potential covariates for the same characteristic (e.g., group size), the covariate included in the univariate model with the lowest AIC value was carried through to the next round of variable selection and all of the related covariates were omitted from the rest of the analysis.

For each aircraft type, a single best model was selected based on AIC. If a model with fewer covariates was within 2 AIC units of the model with the lowest AIC, the simpler model was chosen as the final model.

Transect Detection Probability, $\widehat{P_0}$

An estimate of transect detection probability, $\widehat{P_0}$, was derived using mark-recapture distance-sampling (mrds) methods in the R package mrds (Laake et al. 2016) using visual line-transect survey data and imagery from one Turbo Commander aircraft (Fig. 2). This $\widehat{P_0}$ was used as the transect detection probability correction factor for both aircraft types. In the mrds analysis, the mark-recapture model implemented trial configuration with the assumption of point independence and an exponential distribution; the distance-sampling model used a hazard-rate key function.

Data used to build the mrds model were limited to the visual line-transect data and imagery collected on ASAMM survey flights during which the belly port camera was operational (Fig. 2). Sightings detected in imagery and by ASAMM observers within the left-truncation distance of the Turbo Commander (the strip ranging from 0 to 75 m on either side of the transect) were excluded from the mrds analysis. Due to limited sample sizes in the imagery, all sightings of large cetaceans were incorporated into the mrds model. The large cetacean species detected in the observer and imagery data included bowhead whales, humpback whales

(*Megaptera novaeangliae*), fin whales (*Balaenoptera physalus*), and gray whales (*Eschrichtius robustus*). The typical sighting cue for gray whales is a conspicuous mud plume at the surface of the water. Therefore, we investigated whether incorporating a binary covariate to distinguish gray whales from other large whale species improved the mark-recapture and distance-sampling components of the mrds model.

Availability Bias Correction Factor, $\widehat{P_A}$

The probability that an aerial observer will detect a cetacean during aerial line-transect surveys is a function of the length of time the observer has to detect the animal. Failing to account for the animal's surface and dive durations or the observer's field of view leads to availability bias in estimated density or abundance (Laake and Borchers 2004).

The state model for availability can be represented as the probability that an animal will surface within detectable range (Laake et al. 1997):

$$\widehat{P}_a(y) = \frac{E(s)}{E(s)+E(d)} + \frac{E(d)\left[1-exp\left\{-\frac{\widehat{T(y)}}{E(d)}\right\}\right]}{E(s)+E(d)} \quad [1]$$

where

y: perpendicular distance to the aircraft;

$\widehat{T(y)}$: estimated length of time in which the ocean at perpendicular distance y is in the observer's view; this parameter is a function of the observer's field of view and aircraft speed;

E(s): expected surface duration; and

E(d): expected dive duration.

For estimates of E(s) and E(d), we used the corresponding mean surface and mean dive duration estimates for undisturbed bowhead whales in the southern Beaufort Sea from Robertson et al. (2015). We estimated $\widehat{T(y)}$ using data from field-of-view trials described below and comprehensively detailed in Clarke et al. (2020).

The availability bias correction factors used in the abundance estimate were derived separately for each region and aircraft as a weighted average of the $\hat{P}_a$ at the aircraft's left-truncation distance for bowhead whales in five different activity states designated in Robertson et al. (2015):

$$\hat{P}_{A,aircraft,reg}\left(y_{ltrnc,aircraft}\right) = \sum_{activity\ states} \frac{n_{reg,activity}}{n_{reg}} \hat{P}_{a,aircraft,activity}\left(y_{ltrnc,aircraft}\right), \quad [2]$$

where

$n_{reg,activity}$: number of bowhead whale sightings in region reg in a given activity state;

n_{reg}: total number of bowhead whale sightings in region reg.

Note that the subscript used here (Eqn. 2) for availability is a capital "A" to distinguish this weighted average availability bias correction factor from the parameter $\hat{P}_{a,aircraft,activity}$ representing the availability bias correction factor for a specific combination of aircraft and activity state, which was defined in Eqn. 1.

The five activity states used to categorize each sighting were cow with calf; travel; shallow feeding (≤ 20 m); deep feeding (> 20 m); and socializing. A sighting with a calf was designated as "cow with calf". Although "cow with calf" is not strictly an activity state, the presence of a calf does affect surface and dive durations and we refer to this category as an activity state for simplicity. We assigned bowhead whale sightings that were recorded as "milling" to one of the two feeding categories, depending on the associated water depth. The socializing category comprised sightings recorded as "SAG" in the database. Bowhead whale sightings without calves that were not feeding or socializing were considered to be traveling. Each activity state was assigned the corresponding value of E(s) and E(d) for undisturbed bowhead whales from Robertson et al. (2015).

FOV models

Time-in-view at perpendicular distance y, T(y), increases linearly with viewing distance along the transect (x) as a function of aircraft speed. FOV models were defined using viewing distance rather than time as the response variable so that the results would be applicable at any aircraft speed.

Due to the short viewing distance near the aircraft and the considerable variability in the FOV data, viewing distance at the left-truncation distance was estimated from separate linear models of FOV for each aircraft. Previous authors (Robertson et al. 2015, Ganley et al. 2019) created linear fixed-effects models for forward and aft FOVs separately, enabling estimation of the forward and aft angles and intercepts (Fig. 5). We focus here on models for forward viewing distance, although we also created models for aft and total viewing distance.

The forward field of view is the relevant parameter for deriving an availability bias correction factor for ASAMM data because sightings initially detected in the aft field of view are considered to have been "missed" by the ASAMM primary observers and were excluded from the abundance estimate analysis.

The FOV models were based on scaled perpendicular distance to the transect, pdist.scl, which was computed separately for each aircraft:

$$pdist.scl_{h,l} = \frac{(pdist_{h,l} - \overline{pdist_l})}{\sigma_{pdist_l}}, \quad [3]$$

where

h: waypoint;

l: side of plane (SOP, used only for the Turbo Commander; both sides were pooled for the Twin Otter);

$\overline{pdist_l} = \frac{1}{n_l}\sum_{h \in l} pdist_{h,l}$;

n_l: number of waypoints for SOP *l*; and

σ_{pdist_l}: standard deviation among *pdist* values for SOP *l*.

Twin Otter

Only two primary observers flew in the Twin Otter and sample sizes from the FOV trials were limited due to logistical constraints; therefore, data from both observers on the Twin Otter were pooled in the FOV model for this aircraft. Furthermore, the left and right bubble windows in the Twin Otter were identical in size and placement, so data from both sides of the aircraft were pooled. A single linear model defining the FOV for the aircraft was created:

$$x_k = \gamma + \beta_{pdist.scl} * pdist.scl_k + \varepsilon_k \,, \quad [4]$$

where

x: viewing distance (in meters) along the transect;

k: replicate;

γ: intercept;

$\beta_{pdist.scl}$: fixed effect of *pdist.scl* on slope;

$\varepsilon_k \sim N(0, \sigma^2_{resid})$.

Turbo Commander

In the Turbo Commander, the left window differed slightly from the right window, so separate analyses were conducted for the left and right fields of view. Preliminary analyses suggested that viewing distance along the transect varied among observers. Numerous observers flew ASAMM surveys and five observers flew FOV trials in the Turbo Commander; therefore, observer ID was incorporated as a random effect for the Turbo Commander FOV models. Preliminary investigation of the Turbo Commander FOV data suggested that observer ID did not affect the slopes of the lines for forward field of view; therefore, a random effect for observer ID was incorporated only into the intercepts of each model. The linear mixed effects model of along-transect viewing distance was defined as

$$x_{i,k,l} = \gamma_l + \alpha_{obs,l}[i] + \beta_{pdist.scl,l} * pdist.scl_{i,k,l} + \varepsilon_{i,k,l} \,, \quad [5]$$

where

$\beta_{pdist.scl,l}$: fixed effect of *pdist.scl* on slope for SOP *l*

$\alpha_{obs,l}[i] \sim N\left(0, \sigma^2_{obs,l}\right)$

$\varepsilon_{i,k,l} \sim N\left(0, \sigma^2_{resid,l}\right)$.

One observer flew FOV trials in the Turbo Commander in both 2018 and 2019. Preliminary investigation of the results for this observer suggested that, for a given side of the aircraft, her field of view was quite different each year. This could be due to differences in environmental conditions between the trial periods that could not be controlled for either in the field or analytically. Therefore, this observer's data from 2019 was incorporated into the model as a "new" observer.

Abundance Estimation

Abundance was estimated with a Horvitz-Thompson-like estimator, similar to what is implemented by the dht function in the mrds package (Laake et al. 2016), although modified to account for the variable perpendicular visibility distance encountered during these surveys. Estimated abundance for each region was

$$\widehat{N}_{reg} = \frac{A_{reg}}{a_{reg}} \sum_{aircraft} \sum_{i=1}^{n_{aircraft,reg}} \frac{S_i}{\widehat{P_0} \cdot \hat{P}_{A,aircraft,reg} \cdot \widehat{P_i}}, \quad [6]$$

where

S_i: group size of sighting i from the aircraft in the region;

A_{reg}: total area (km^2) of the region;

a_{reg}: area (km^2) surveyed by both types of aircraft in the region. This was computed as

$$a_{reg} = 2\sum_v L_{v,ott,reg} w_v + 2\sum_v L_{v,cmdr,reg} w_v \,, \quad [7]$$

where

L_v: length (km) of transect and CAPs passing survey effort flown by the aircraft in the region under visibility conditions v (defined in the Detection Functions section above);

w_v: perpendicular visibility distance (km) averaged across both sides of the aircraft. This was computed for each record in the ASAMM database by first converting the categorical variables for perpendicular visibility on each side of the aircraft into integer-valued distances as defined in the Detection Functions section above, then averaging the values from both sides;

$\widehat{P_0}$: estimated transect detection probability;

$\hat{P}_{A,aircraft,reg}$: estimated weighted average availability bias correction factor for the aircraft in the region; and

$\widehat{P_i}$: estimated average detection probability of an available whale, assuming P_0=1.0 and the observation-specific right-truncation distance is $w_{v,i}$.

$$\widehat{P_i} = \frac{1}{w_{v,i}} \int_{y_{ltrnc,aircraft}}^{w_{v,i}} g(y,z)dy.$$

Total estimated abundance was computed as the sum of the regional estimates:

$$\widehat{N_{tot}} = \widehat{N_{AG}} + \widehat{N_{EBS}} + \widehat{N_{WBS}} \,. \quad [8]$$

Uncertainty Estimation and Sensitivity Analyses

Uncertainty estimates and sensitivity analyses were conducted using a bootstrap algorithm that incorporated both parametric and non-parametric sampling. See Appendix for pseudocode for the bootstrap algorithm. The bootstrap algorithm generated samples to estimate uncertainty in estimates of the following parameters: $\hat{T}_{aircraft}(y_{ltrnc,aircraft})$, $\hat{P}_0$, $\hat{P}_{i,aircraft}$, $\hat{P}_{A,aircraft,reg}$, $\hat{N}_{reg}$, and $\hat{N}_{tot}$. Bootstrap 95% confidence intervals for strata and total abundance estimates were derived using the percentile method.

A key feature of the bootstrap algorithm is that it attempted to maintain consistency in sample size, by region and aircraft type, for each component of the analysis. Sample units used in the analysis have unique sample labels. Sample units and sample labels are specified by the combination of aircraft type, survey year, and transect number. For $\hat{T}_{aircraft}(y_{ltrnc,aircraft})$, the bootstrap algorithm sampled individual trials (flights down the FOV transect) with replacement, ensuring that the number of bootstrap trials for each aircraft equaled the actual number flown during the field experiments. For $\hat{P}_0$, the bootstrap algorithm sampled units (with replacement) from the subset of ASAMM flights in 2018 and 2019 conducted with the belly port camera during which large cetaceans were sighted. For $\hat{P}_{i,aircraft}$ and $\hat{P}_{A,aircraft,reg}$, the bootstrap algorithm sampled units (with replacement) for each region (separately for each aircraft), ensuring that the number of bootstrap sample units per region and aircraft equaled the number flown during the August 2019 surveys. Because the model used to derive $\hat{P}_i$ for the Turbo Commander incorporated sightings from surveys on the Turbo Commander from 2009 to 2019, the bootstrap algorithm sampled units (with replacement) from Turbo Commander flights beginning in 2009 to ensure that the total number of bootstrap sample units used to create the

bootstrap mcds model was not less than the actual number of sample units used to create the original mcds model. The algorithm ran a total of 10,000 iterations.

To determine which components of the analysis contributed the most to the overall uncertainty in $\widehat{N}_{\text{reg}}$ and $\widehat{N}_{\text{tot}}$, the bootstrap algorithm was run sequentially, holding one parameter fixed at its point estimate during each run. The parameters that were tested were P_0 (transect detection probability), $P_{A,cmdr}$ (availability bias correction factor for the Turbo Commander; fixed across all regions simultaneously), and $P_{A,ott}$ (availability bias correction factor for the Twin Otter; fixed across all regions simultaneously). Lastly, to examine the effects of the inherent variability in the line-transect survey data (i.e., variability across transects), the algorithm ran with the survey effort and sighting data held fixed and the estimated parameters randomly sampled in each iteration. A total of 10,000 iterations were run in the sensitivity analysis for each parameter.

Bootstrap uncertainty estimates and sensitivity analyses omitted all iterations in which the abundance estimate for any single stratum was zero. We saw bowhead whales in all strata during August 2019, so a bootstrap sample with a stratum abundance estimate of zero is outside the relevant domain for the abundance estimate.

RESULTS

August 2019 Bowhead Whale Abundance Survey

During the August 2019 bowhead whale abundance survey, bowhead whale distribution and density largely matched expectations based on all available information, including Indigenous knowledge, historical whaling records, previous aerial surveys, and telemetry

studies. However, there were some notable exceptions, represented by the sightings offshore of the blue polygons in the Beaufort Sea in Figure 1. Table 2 provides sighting and effort summaries, by region and aircraft. The highest bowhead whale densities were observed in the eastern Beaufort Sea, where all three CAPs sessions of the survey period occurred. Amundsen Gulf had the lowest observed bowhead whale densities. Most bowhead whale sightings were well within the survey area boundaries (Fig. 1).

A total of five sightings of single large cetaceans could not be identified to species, four in the eastern Beaufort Sea and one in the western Beaufort Sea.

Gray whales were the only other large cetaceans identified to species during the August 2019 bowhead whale abundance survey period. No other species of large cetaceans were expected to be encountered. The gray whales were observed during only one flight, on the Twin Otter, on 21 August. There were 8 gray whale sightings, totaling 15 whales, including 1 calf. The gray whales were observed feeding north of the Tuktoyaktuk Peninsula in 30-55 m deep water.

Belly Port Imagery

In 2018 and 2019 combined, a total of 477,490 images were collected (167,862 in 2018 and 309,628 in 2019) and 106,901 were analyzed (33,519 from 2018 and 73,382 from 2019). On average, the photo analyst could review 133 images per hour; therefore, images from one survey hour required approximately 3.4 hours of photo analyst time to review.

Detection Functions

The final mcds detection function model for the Twin Otter incorporated only a single scale covariate, survey altitude (Table 3). The coefficient for altitude was negative, implying that detection probability decreased with increased survey altitude.

The final mcds detection function model for the Turbo Commander incorporated three scale covariates: survey altitude, sea ice cover, and Beaufort Sea State (Table 3). In contrast to the Twin Otter detection function model, the coefficient for altitude in the Turbo Commander model was positive, implying that detection probability increased with increased survey altitude in the Turbo Commander. Heavier sea ice coverage and higher sea states decreased detection probability.

The reason for the opposite signs for the altitude coefficients in the Twin Otter and Turbo Commander mcds detection function models is unknown. The range and distribution of altitude values used to build the models for both aircraft were similar: the minimum/mean/maximum values for the Twin Otter were 961 ft / 1,231 ft / 1,843 ft and for the Turbo Commander were 918 ft / 1,388 ft / 1,906 ft. The standard error of the altitude parameter for the Twin Otter (0.913; Table 3) was considerably larger than for the Turbo Commander (0.166; Table 3). It is possible that the smaller sample size available to build the Twin Otter model (64 sightings) compared to the Turbo Commander model (1,838 sightings) affected our ability to identify covariates that were directly related to differences in detection probability among sightings by observers aboard the Twin Otter.

Transect Detection Probability, $\widehat{P}_0$

The $\hat{P}_0$ analysis used a total of 402 observations from the ASAMM observers and imagery combined; 390 observations were detected by the ASAMM observers; 12 imagery sightings were missed by the ASAMM observers; 72 observations were detected in the imagery; and 60 observations were detected by both the ASAMM observers and in the imagery. The ASAMM line-transect data comprised 290 bowhead whale, 76 gray whale, 20 humpback whale, and 4 fin whale sightings (Table 4). The imagery comprised 54 bowhead whale, 17 gray whale, and 1 humpback whale sighting (Table 4).

The total AIC for the mrds model with the species covariate was 2.5 units higher than the null model. Furthermore, the coefficient for the species covariate was between 0 and 1 in both the distance-sampling and the mark-recapture components of the mrds model. Therefore, the species covariate was not included in the final mrds model used to estimate P_0.

Transect detection probability was estimated to be 0.727, with a bootstrap CV of 0.149 (Table 2). Figure 6 shows the sampling distribution for $\hat{P}_0$ generated using the bootstrap algorithm.

FOV Trials

One FOV flight was flown in the Twin Otter with two ASAMM observers over a target near Inuvik on 22 August 2019. Survey conditions included partly cloudy to overcast skies, with unlimited visibility and no impediments to visibility.

FOV flights were flown in the Turbo Commander with a total of five ASAMM observers over the Franklin Bluffs target on 18 and 19 September 2018, and 7 September 2019. Survey conditions during the flights in 2018 included clear skies, unlimited visibility, and no

impediments to visibility. Survey conditions during the flight in 2019 included partly cloudy skies, unlimited visibility, and no visual impediments. The east/west transects located south of the target were flown for all trials to minimize effects of crabbing (i.e., wind pushing the aircraft sideways) and to keep the sun's glare at the observers' backs.

FOV Models

Twin Otter

FOV data and the resulting model of viewing distance suggested that the target remained in view longer from the farthest (2,000 m perpendicular distance) transect compared to the closest (500 m perpendicular distance) transect. The estimated intercept was at 2,180.5 (SE = 169.9), and the estimated slope was 131.7 (SE 175.5). The model estimated that a target located at the left-truncation distance (350 m) was visible to an observer on the Twin Otter for approximately 35 seconds.

Turbo Commander

Although there was variability in the forward field of view among observers, the models suggested that the target remained in view longer from the 2,000-m transect compared to the 500-m transect. Model results are provided in Table 5. The model estimated that a target located at the left-truncation distance (75 m) was visible to an observer on the Turbo Commander for approximately 69 seconds.

Availability Bias Correction Factors, $\widehat{P}_{A}$

The proportion of bowhead whale sightings in each of the five activity states differed by aircraft and region. In Amundsen Gulf, both bowhead whale sightings were traveling. In the eastern Beaufort Sea, the Twin Otter observed 42.1% of the bowhead whale sightings in cow-calf pairs, 56.1% traveling, and 1.8% feeding in shallow water; the Commander observed 15.9% in cow-calf pairs, 80.7% traveling, and 3.4% feeding in shallow water. In the western Beaufort Sea, the Commander observed 91.7% of the bowhead whale sightings traveling and 8.3% feeding in shallow water.

The availability bias correction factors and associated CVs are provided in Table 2. In general, $\hat{P}_{A}$ was higher for the Turbo Commander than the Twin Otter. $\hat{P}_{A}$ and CV($\hat{P}_{A}$) were similar between regions for each aircraft type.

Abundance and Uncertainty Estimates

The regional abundance estimate for Amundsen Gulf was 275 whales (CV = 0.550; bootstrap 95% CI [83, 654], Table 2; Fig. 7), the eastern Beaufort Sea was 13,207 whales (CV = 0.570; bootstrap 95% CI [7,108, 27,522], Table 2; Fig. 8), and the western Beaufort Sea was 1,049 whales (CV = 0.538; bootstrap 95% CI [252, 2,132]; Table 2, Fig. 9). The total abundance estimate for the BCB bowhead whale population was 14,531 whales (CV = 0.540; bootstrap 95% CI [7,968, 29,376]; Table 2, Fig. 10).

Results from the bootstrap algorithm used to estimate uncertainty in the regional and total abundance estimates provide insight into the largest sources of uncertainty. Resampling the line-transect survey data (effort and sightings, by sample unit) resulted in 971 iterations

with abundance estimates equal to zero for Amundsen Gulf and 2 iterations with abundance estimates equal to zero for the western Beaufort Sea. None of the iterations resulted in zero abundance for the eastern Beaufort Sea. However, line-transect sampling variability within the eastern Beaufort Sea contributed heavily to uncertainty in the total abundance estimate by producing extremely large outliers in regional abundance, as explained further below.

To examine the source of outliers in the bootstrap estimates of total abundance, we first subjectively defined an outlier to be any estimate more extreme than 1.75 times the inter-quartile range:

$$\widehat{N}_b < \widehat{N}_{1Q} - 1.75 * IQR$$

or

$$\widehat{N}_b > \widehat{N}_{3Q} + 1.75 * IQR\ , \qquad [9]$$

where

$\widehat{N}_b$: total abundance estimate from bootstrap iteration *b*;

$\widehat{N}_{1Q}$: first quartile of bootstrap total abundance estimates;

$\widehat{N}_{3Q}$: third quartile of bootstrap total abundance estimates; and

IQR: inter-quartile range, defined as $\widehat{N}_{3Q} - \widehat{N}_{1Q}$.

Using this definition, all outliers corresponded to bootstrap abundance estimates that were too large. Next, we visually compared the bootstrap distributions of $\hat{P}_0$, $\hat{P}_{A,aircraft,reg}$, $\hat{T}_{aircraft}\left(y_{ltrnc,aircraft}\right)$ (time-in-view at the left-truncation distance), and $n_{aircraft,reg}$ (number of sightings) for the subset of bootstrap iterations that produced outliers in total abundance versus the subset that did not produce outliers. The number of bootstrap sightings for the Twin Otter in the eastern Beaufort Sea region clearly was the source of outliers in bootstrap total

abundance estimates (Fig. 11). Furthermore, omitting outliers (Eqn. 9) reduced the bootstrap $\widehat{CV}\left(\widehat{N_{tot}}\right)$ from 0.540 to 0.289.

Sensitivity Analyses

Results of the bootstrap sensitivity analyses are provided in Table 6. The bootstrap analysis conducted with $\hat{P}_0$ fixed at the point estimate resulted in a decrease in CV($\widehat{N}$) of 0.15 compared to the base model. There was essentially no difference in the estimated CV($\widehat{N}$) when the $\hat{P}_{A,aircraft,reg}$ for either aircraft were fixed at their point estimates compared to the base model. The bootstrap analysis conducted with fixed line-transect survey data resulted in a decrease in CV($\widehat{N}$) of 0.22 compared to the base model, reinforcing the finding mentioned above that line-transect sampling variability contributed heavily to the uncertainty in the total abundance estimate.

DISCUSSION

We estimated the BCB bowhead whale population to be 14,531 whales (CV = 0.540; bootstrap 95% CI [7,968, 29,376]) in 2019. This estimate is based on aerial line-transect surveys during August 2019 across the population's primary summer range in the Beaufort Sea shelf and Amundsen Gulf. During the survey period, bowhead whale density varied spatially between and within the three geographic strata used in the analysis. The highest density and the greatest abundance were in the eastern Beaufort Sea and lowest density and abundance in Amundsen Gulf.

The whales' August distribution and density in the study area in 2019 was similar to previous years based on all available information from Indigenous knowledge, historical whaling records, previous aerial surveys, and telemetry studies, although there were two notable exceptions. First, Clarke et al. (2020) found that the bowhead whale distribution in the western Beaufort sea was farther from shore during summer (July and August combined) 2019 compared to summer 2012-2018. Second, Clarke et al. (2020) also reported that the areas of highest relative density near the Tuktoyaktuk Peninsula in 2019 were farther from shore and in deeper water (51-2000 m depth) compared to 2007-2009, when Harwood et al. (2010) found greatest densities in waters 20-50 m deep.

Deriving an estimate of absolute population abundance for BCB bowhead whales from line-transect surveys is complicated due to four fundamental factors: 1) the population's entire summer range stretches from Chukotka, Russia, across the Beaufort Sea to Amundsen Gulf and Viscount Melville Sound; 2) the spatial extent of the August 2019 survey area was vast, imposing logistical constraints on aerial survey design and implementation that affected data collection; 3) correction factors for transect detection probability and availability bias (requiring estimates of observer field of view and bowhead whale surface duration and dive duration) are needed; and 4) considerable spatial heterogeneity in the line-transect data (i.e., variable bowhead whale encounter rates across transects) exist due to variability in the ecosystem and weather during the period of the abundance survey. Below, we discuss the influence of each of these factors on the abundance estimate.

The first caveat with the present abundance estimate is that the entire summer range of BCB bowhead whales was not included within the August 2019 survey area. A small number of

bowhead whales have been known to occur off Chukotka, Russia, during August (Citta et al. 2021). Because the whales off Chukotka are thought to represent only a very small proportion of the overall population, and because of logistical constraints, the survey area excluded waters off Chukotka. The inability to base a survey team out of Ulukhaktok for the duration of the survey period due to lack of aviation fuel in the village resulted in limited survey coverage in Amundsen Gulf and off the west coast of Banks Island. This issue also precluded our ability to conduct a scouting flight to Viscount Melville Sound. However, the surveys that were conducted in Amundsen Gulf and all available knowledge on bowhead whale distribution in the region suggests that Amundsen Gulf is not a high-density area for bowhead whales. Similarly, all available knowledge suggests that the waters off the west coast of Banks Island and in Viscount Melville Sound do not typically have high densities of BCB bowhead whales. If significant numbers of BCB bowhead whales were distributed in areas outside the analysis area during August 2019, the present abundance estimate would be biased low.

The need to estimate correction factors for perception bias and availability bias is a complication that is common to all analyses used to estimate cetacean abundance from strip- or line-transect survey data, regardless of survey platform (vessel or aircraft) and observer type (e.g., human, imagery, or acoustic): no detection method is infallible and cetaceans cannot always be seen or heard. For the present analysis, the transect detection probability estimate, $\hat{P}_0$, for the Turbo Commander was applied to the data from both aircraft types, and the total sample size of large cetacean detections in the imagery was relatively small. These issues resulted from logistical constraints and the considerable amount of time required to manually process imagery from the belly port camera. The bubble windows in the Twin Otter were

smaller than in the Turbo Commander and the former had a larger left-truncation distance. It is possible that the true P_0 for the Twin Otter could have been less than the value used in this analysis. If that were the case, the present abundance estimate would be biased low. For example, if P_0 for the Twin Otter were 0.6 instead of the assumed value 0.727, the total abundance estimate would have been 16,063 whales instead of 14,531 whales.

Furthermore, the sensitivity analysis suggested that decreasing the uncertainty in $\hat{P}_0$ could profoundly reduce the uncertainty in the overall abundance estimate. Using aircraft that were all identically configured would simplify analyses and would likely improve accuracy and precision of abundance estimates derived from aerial line-transect surveys because the sample sizes used to estimate transect detection probability and to construct the distance-sampling component of the detection function model would increase. Additionally, collection of additional imagery data concurrent with future line-transect surveys and development of reliable algorithms to automatically detect large cetacean sightings in imagery would undoubtedly expedite the imagery review process, ultimately resulting in more precise estimates of transect detection probability and abundance as sample size increases.

Bowhead whale surface intervals and dive intervals are known to vary widely depending on activity state, group size and composition, and habitat (e.g., Dorsey et al. 1989, Wursig and Clark 1993, Robertson et al. 2013, Wursig and Koski 2021). We assumed that bowhead whale surface and dive durations were known constants in the availability bias estimator, resulting in an overestimate of precision. Additional information on bowhead whale surface and dive durations, and associated variability, would benefit any analysis that requires estimates of

availability to surface (e.g., humans or imagery) or underwater (e.g., passive acoustic monitoring) “observers”.

We derived region-specific estimates of availability bias, weighted by the proportion of bowhead whale sightings categorized into five activity states. The precision in the estimate of total abundance may be improved by eliminating the regional stratification from the availability bias estimator, thereby relying on observation-specific availability correction factors.

Due to the very small number of large whale sightings that could not be positively identified to species (n = 5 during August 2019), we did not incorporate a species-identification bias correction factor into the present analysis. It is highly likely that those five whales were bowhead whales because other large cetaceans rarely venture into the survey area during summer and autumn. However, ASAMM’s sightings of gray whales off the Tuktoyaktuk Peninsula in August 2019 reinforces the idea that not all large cetaceans read the rule book. If those five “unidentified large cetacean” sightings were bowhead whales, the present abundance estimate would be biased slightly low.

This analysis used geographically stratified mark-recapture distance sampling methods to estimate abundance. The analysis used a combination of parametric and non-parametric bootstrap methods to estimate uncertainty in the parameter estimates and sensitivity of the precision of the abundance estimate to the precision of the parameter estimates. The bootstrap analyses suggested that precision in the abundance estimate could be increased by using spatially-explicit modeling techniques to address the variability among samples (transects) in the line-transect data. When we omitted bootstrap iterations that produced extreme outliers in total abundance, CV($\widehat{N}$) dropped from 0.540 to 0.289. Admittedly, our

definition of outliers was subjective. However, this result suggests that explicitly addressing the spatial variability in bowhead whale distribution at sub-stratum scales holds considerable promise in increasing the precision of the estimate of total abundance.

The Alaska Eskimo Whaling Commission and NOAA, partners who co-manage the BCB bowhead whale population, are interested in the best option(s) for estimating abundance of this population in the future. The spring ice-based survey as the whales round Point Barrow has been incredibly successful in the past, producing abundance estimates with tight confidence intervals (Givens et al. 2016, 2020, 2021). Unfortunately, spring ice conditions are deteriorating, resulting in elevated risks to human safety and logistical challenges. Aerial photo-identification data have also been successfully used to estimate abundance of this population (Givens et al. 2018). However, the complete photo mark-recapture effort, from field work to completion of the final abundance estimate, is costly and time-consuming, and the existing bowhead whale matching process requires specific experience matching images from the existing library.

The abundance estimate presented here is smaller and less precise than Givens et al.'s (2016) abundance estimate from the 2011 ice-based survey, which was 16,820 whales with a CV of 0.052. The present abundance estimate is slightly larger, but also less precise, than Givens et al.'s (2020, 2021) abundance estimate from the 2019 ice-based survey: 14,025 (CV = 0.228). Currently under investigation are a number of analytical refinements, including those listed above, that we believe should be applied to the existing data to address issues of bias and improve precision in the abundance estimate. Ultimately, we believe aerial line-transect surveys will provide an accurate and unbiased estimate of population abundance necessary to effectively manage BCB bowhead whales.

ACKNOWLEDGMENTS

We are very grateful to Billy Adams, Craig George, and Robert Suydam at the North Slope Borough (NSB) Department of Wildlife Management for their assistance with survey planning and outreach. Geof Givens and Dave Miller helped with both pre- and post-survey methods development. The 2019 field season was funded, in part, by the US Department of the Interior (USDOI), BOEM, Environmental Studies Program, Washington, D.C., through Interagency Agreement No. M17PG00031 with the Alaska Fisheries Science Center (AFSC), NOAA. We are eternally grateful to BOEM for providing funding to arctic marine mammal monitoring and ecological research for 41 years, and particularly to Cathy Coon and Rick Raymond for overseeing the project during the 2019 field season. NOAA-AFSC provided partial funding to enable the extension of the normal ASAMM study area to include the eastern Beaufort Sea shelf and Amundsen Gulf. Thank you NSB Mayor Harry Brower, Jr. for sharing thoughtful insights about the arctic ecosystem and communities, and for your forward-thinking prioritization of long-term monitoring of arctic marine mammals. The Alaska Eskimo Whaling Commission provided welcome enthusiasm and support to our survey teams, and that was especially heartening during the first week of the August 2019 field season when low ceilings, fog, and wind-curtailed survey efforts. The field teams during the August surveys were exceptional in every way, and included team leaders Amelia Brower, Janet Clarke, Megan Ferguson, Katie Jackson, and Amy Willoughby, and observers Corey Accardo, Lisa Barry, Laura Ganley, Suzie Hanlan, Rachel Hardee, Richard Holt, and Nick Metheny. Clearwater Air, Inc., safely, professionally, and successfully provided aircraft support to ASAMM from 2009 to 2019, and we are especially grateful to Stan Churches, Andy Harcombe, and Jake Turner for their

dedication to ASAMM; the 2019 project was funded via Contract No. D15PC00102 with USDOI. The Twin Otter aircraft, pilots, and mechanical support were provided by Kenn Borek Air, Ltd., and Aklak Air via Contract No. 140D8119C0004 with USDOI. Mike Hay from XeraGIS developed and maintained the ASAMM Survey data collection and post-processing software; Mike was always available to help fix things that our team broke in the field. Ben Hou from AFSC was instrumental in helping ASAMM develop imagery protocols. Real-time flight following was provided by U.S. Department of the Interior, Bureau of Land Management, Alaska Interagency Coordination Center, South Zone Dispatch, and Kenn Borek Dispatch. Multiple entities in Canada helped us get off the ground in foreign territory: Canada Department of Fisheries and Oceans, Fisheries Joint Management Committee Canada, and Inuvialuit Game Council. We appreciate the assistance and guidance of Julie Speegle (NOAA Public Affairs Officer), Maggie Mooney-Seus (AFSC Communications Program Manager), John Callahan (BOEM Public Affairs Officer), and Maureen Clark (U.S. Fish and Wildlife Service Public Affairs Officer) on media relations. Geof Givens, Kim Goetz, Paul Conn, and Jim Lee provided useful feedback on previous drafts of this manuscript. Of course, we thank the dogs of ASAMM, the most loyal supporters of all.

CITATIONS

ASAMM. 2019. Aerial Surveys of Arctic Marine Mammals Observer Manual 2019 v.10. Unpubl. manuscr., 272 p. Available Marine Mammal Laboratory, Alaska Fisheries Science Center, 7600 Sand Point Way NE, Seattle, WA 98115.

Bates, D., M. Maechler, B. Bolker, and S. Walker. 2015. Fitting linear mixed-effects models using lme4. J. Stat. Software 67(1):1-48. doi:10.18637/jss.v067.i01.

Bivand, R. and N. Lewin-Koh. 2019. maptools: Tools for Reading and Handling Spatial Objects. R package version 0.9-9. Available from: https://CRAN.R-project.org/package=maptools.

Bivand, R., and C. Rundel. 2019. rgeos: Interface to Geometry Engine - Open Source ('GEOS'). R package version 0.5-2. Available from: https//CRAN.R-project.org/package=rgeos.

Bivand, R. S., E. J. Pebesma, and V. Gomez-Rubio. 2013. Applied Spatial Data Analysis with R, Second Edition. Springer, NY. Available from: http://www.asdar-book.org/.

Bivand, R., T. Keitt, and B. Rowlingson. 2019. rgdal: Bindings for the 'Geospatial' Data Abstraction Library. R package version 1.4-8. Available from: https://CRAN.R-project.org/package=rgdal.

Braund S. R. and Associates. 2018. Description of Alaskan Eskimo bowhead whale subsistence sharing practices. Report to the Alaska Eskimo Whaling Commission, 74 p. Available Alaska Eskimo Whaling Commission, P.O. Box 570, Utqiaġvik, AK 99723.

Buckland, S. T., D. R. Anderson, K. P, Burnham, J. L. Laake, D. L. Borchers, and L. Thomas. 2001. Introduction to Distance Sampling: Estimating Abundance of Biological Populations. Oxford Univ. Press, Oxford. 432 p.

Citta, J. J., L. Quakenbush, and J. C. George. 2021. Distribution and behavior of Bering-Chukchi-Beaufort bowhead whales as inferred by satellite telemetry, p. 31-56. *In*: J.C. George and J.G.M. Thewissen (editors), The Bowhead Whale *Balaena mysticetus*: Biology and Human Interactions. Academic Press, London.

Clarke, J. T., A. A. Brower, M. C. Ferguson, and A. L. Willoughby. 2019. Distribution and relative abundance of marine mammals in the eastern Chukchi and Western Beaufort seas, 2018. Annual Report, OCS Study BOEM 2019-021. Marine Mammal Laboratory, Alaska Fisheries Science Center, NMFS, NOAA, 7600 Sand Point Way NE, Seattle, WA 98115-6349.

Clarke, J. T., A. A. Brower, M. C. Ferguson, A. L. Willoughby, and A. D. Rotrock. 2020. Distribution and relative abundance of marine mammals in the eastern Chukchi Sea, eastern and western Beaufort Sea, and Amundsen Gulf, 2019. Annual Report, OCS Study BOEM 2020-027. Marine Mammal Laboratory, Alaska Fisheries Science Center, NMFS, NOAA, 7600 Sand Point Way NE, Seattle, WA 98115-6349.

da Silva, C. Q., J. Zeh, D. Madigan, J. Laake, D. Rugh, L. Baraff, W. Koski, and G. Miller. 2000. Capture-recapture estimation of bowhead whale population size using photo-identification data. J. Cetacean Res. Manage. 2(1):45-61.

Dorsey, E. M., W. J. Richardson, and B. Würsig. 1989. Factors affecting surfacing, respiration, and dive behaviour of bowhead whales, *Balaena mysticetus*, summering in the Beaufort Sea. Can. J. Zool. 67(7):1801-1815. doi:10.1139/z89-257.

Ganley, L. C., S. Brault, and C. A. Mayo. 2019. What we see is not what there is: Estimating North Atlantic right whale *Eubalaena glacialis* local abundance. Endang. Species Res. 38:101-113.

George, J. C., J. Bada., J. Zeh, L. Scott, S. E. Brown, T. O'Hara, and R. Suydam. 1999. Age and growth estimates of bowhead whales (*Balaena mysticetus*) via aspartic acid racemization. Can. J. Zool. 77:571-580.

George, J. C., G. H. Givens, R. Suydam, J. Herreman, J. Mocklin, B. Tudor, R. DeLong, C. Clark, R. A. Charif, and A. Rahaman. 2013. Unpubl. doc. submitted to Int. Whal. Comm. Scientific Committee (SC/65A/BRG11Rev). 25 p.

George, J. C., J. G. M. Thewissen, A. Von Duyke, G. A. Breed, R. Suydam, T. L. Sformo, B. T. Person, and H. K. Brower Jr. 2021. Life history, growth, and form, p. 87-115. *In*: J.C. George and J.G.M. Thewissen (editors), The Bowhead Whale *Balaena mysticetus*: Biology and human interactions. Academic Press, London.

Givens, G. H., S. L. Edmondson, J. C. George, R. Suydam, R. A. Charif, A. Rahaman, D. Hawthorne, B. Tudor, R. A. DeLong, and C. W. Clark. 2016. Horvitz-Thompson whale abundance estimation adjusting for uncertain recapture, temporal availability variation, and intermittent effort. Environmetrics 27:134-146. DOI: dx.doi.org/10.1002/env.2379.

Givens, G. H., J. A. Mocklin, L Vate Brattström, B. J. Tudor, W. R. Koski, J. E. Zeh, R. Suydam, and J. C. George. 2018. Survival rate and 2011 abundance of Bering-Chukchi-Beaufort seas bowhead whales from photo-identification data over three decades. Unpubl. doc. submitted to Int. Whal. Comm. Scientific Committee (SC/67b/AWMP/01 Rev1). 24 p.

Givens, G. H., J. C. George, R Suydam, and B. Tudor. 2020. Bering-Chukchi-Beaufort Seas bowhead whale (*Balaena mysticetus*) abundance estimate from the 2019 ice-based survey. Unpubl. doc. submitted to Int. Whal. Comm. Scientific Committee (SC/68B/ASI/02). 18 p.

Givens, G. H., J. C. George, R. Suydam, B. Tudor, A. Von Duyke, B. Person, and K. Scheimreif. 2021. Correcting the 2019 survey abundance of Bering-Chukchi-Beaufort seas bowhead whales for disturbance from powered skiffs. Unpubl. doc. submitted to Int. Whal. Comm. Scientific Committee (SC/68C/ASI/01). 17 p.

Hain, J. H. W., S. L. Ellis, R. D. Kenney, and C. K. Slay. 1999. Sightability of right whales in coastal waters of the southeastern United States with implications for the aerial monitoring program, p. 191-208. *In*: G. W. Garner, S. C. Amstrup, J. L. Laake, B. F. J. Manly, L. L. McDonald, and D. G. Robertson (editors), Marine Mammal Survey and Assessment Methods. Proceedings of the Symposium on Surveys, Status, and Trends of Marine Mammal Populations, Seattle, WA, USA, 25-27 February 1998.

Harwood, L. A., J. Auld, A. Joynt, and S. E. Moore. 2010. Distribution of bowhead whales in the SE Beaufort Sea during late summer, 2007-2009. DFO Can. Sci. Advis. Sec. Res. Doc. 2009/111. iv + 22 p.

Koski, W., J. Zeh, J. Mocklin, A. R. Davis, D. J. Rugh, J. C. George, and R. Suydam. 2010. Abundance of Bering-Chukchi-Beaufort bowhead whales (*Balaena mysticetus*) in 2004 estimated from photo-identification data. J. Cetacean Res. Manage. 11(2):89-99.

Krogman, B. D., D. J. Rugh, R. Sonntag, J. E. Zeh, and D. Ko. 1989. Ice-based census of bowhead whales migrating past Point Barrow, Alaska 1978-1983. Mar. Mammal Sci. 5:116-138.

Laake, J. L. and D. L. Borchers. 2004. Methods for incomplete detection at distance zero, p. 109-189. *In*: S. T. Buckland, D.R. Anderson, K.P. Burnham, J.L. Laake, D.L. Borchers, and L. Thomas (editors), Advanced Distance Sampling: Estimating Abundance of Biological Populations. Oxford University Press, Oxford.

Laake, J. L., J. Calambokidis, S. D. Osmek, and D. J. Rugh. 1997. Probability of detecting harbor porpoise from aerial surveys: estimating *g(0)*. J. Wildl. Manage. 61(1):1997.

Laake, J., D. Borchers, L. Thomas, D. Miller, and J. Bishop. 2016. mrds: Mark-Recapture Distance Sampling. R package version 2.1.17. https://CRAN.R-project.org/package=mrds.

Marques, F. F. C., and S. T. Buckland. 2003. Incorporating covariates into standard line transect analyses. Biometrics 59: 924-935. doi:10.1111/j.0006-341X.2003.00107.x.

Moore, S. E., and R. R. Reeves. 1993. Distribution and movement, p. 313-386. *In*: J. J. Burns, J.J., Montague, and C. J. Cowles, (editors), The Bowhead Whale. Soc. Mar. Mammal., Spec. Publ. No. 2.

Muto, M. M., V. T. Helker, B. J. Delean, R. P. Angliss, P. L. Boveng, J. M. Breiwick, B. M. Brost, M.F. Cameron, P. J. Clapham, S. P. Dahle, M. E. Dahlheim, B. S. Fadely, M. C. Ferguson,L.W. Fritz, R. C. Hobbs, Y. V. Ivashchenko, A. S. Kennedy, J. M. London, S. A. Mizroch,R. R. Ream, E. L. Richmond, K. E. W. Shelden, K. L. Sweeney, R. G. Towell, P. R. Wade, J.M. Waite, and A. N. Zerbini. 2020. Alaska marine mammal stock assessments, 2019. U.S. Dep. Commer., NOAA Tech. Memo. NMFS-AFSC-404, 395 p.

Pebesma, E.J., and R.S. Bivand. 2005. Classes and methods for spatial data in R. R News 5 (2). Available from: http://cran.r-project.org/doc/Rnews/.

Robertson, F. C., W. R. Koski, T. A. Thomas, W. J. Richardson, B. Würsig, and A. W. Trites. 2013. Seismic operations have variable effects on dive-cycle behavior of bowhead whales in the Beaufort Sea. Endang. Species Res. 21(2):143-160.

Robertson, F. C., W. R. Koski, J. R. Brandon, T.A. Thomas, and A. W. Trites. 2015. Correction factors account for the availability of bowhead whales exposed to seismic operations in the Beaufort Sea. J. Cetacean Res. Manage. 15:35-44.

Suydam, R., J. C. George, M. Ferguson, G. Givens, and C. Coon. 2019. Update on plans for a population survey in 2019 of Bering-Chukchi-Beaufort bowhead whales. Unpubl. doc. submitted to Int. Whal. Comm. Scientific Committee (SC/68A/ASW/05). 4 p.

Thomas, L., S. T. Buckland, E. A. Rexstad, J. L. Laake, S. Strindberg, S. L. Hedley, J. R. B. Bishop, T. A. Marques, and K. P. Burnham. 2010. Distance software: design and analysis of distance sampling surveys for estimating population size. J. Appl. Ecol. 47:5–14. doi: 10.1111/j.1365-2664.2009.01737.x .

Willoughby, A., M. Ferguson, B. Hou, C. Accardo, A. Rotrock, A. Brower, J. Clarke, S. Hanlan, M. Foster, K. Pagan, and L. Barry. 2021. Belly Port Camera Imagery Collected to Address Cetacean Perception Bias During Aerial Line-Transect Surveys: Methods and Sighting Summaries. U.S. Dep. Commer., NOAA Tech. Memo. NMFS-AFSC-427, 111 p.

Würsig, B. and C. Clark. 1993. Behavior, p. 157-199. *In*: J. J. Burns, J.J., Montague, and C. J. Cowles, (editors), The Bowhead Whale. Soc. Mar. Mammal., Spec. Publ. No. 2.

Würsig, B. and W. R. Koski. 2021. Natural and potentially disturbed behavior of bowhead whales, p. 339-363. *In*: J.C. George and J.G.M. Thewissen (editors), The Bowhead Whale *Balaena mysticetus*: Biology and Human Interactions. Academic Press, London.

Table 1. --Definitions of covariates considered for inclusion in detection function models for the Twin Otter (o) and Turbo Commander (c) aircraft.

Covariate Name	Definition	Categories	Aircraft
**size*	observed group size of the sighting		o
loggs	$\log_{10}$(*size*)		o,c
***size.scl*	(*size – mean(size))/sd(size)*		c
catsize	categorical group size	{1, >1}	o,c
catsizeGT2	categorical group size	{1, 2, >2}	o,c
***catsize10*	categorical group size	{1, 2, >2 & ≤10, >10}	c
***catsizeGT10*		{≤10, >10}	c
log10z	$\log_{10}$ of the depth of the ocean floor at the location of the aircraft when sighting was abeam		o,c
catZ	categorical variable for depth	{0-20 m, 21-50 m, 51-200 m, 201-2000 m, >2000 m)	o,c
iBeauf	Beaufort sea state, as an integer-valued numeric variable ranging from 1 to 5		o,c
f5Beauf	Beaufort sea state, as a categorical variable	{0 to 2, 3 to 5}	o,c
Long100	longitude of the sighting, scaled by -1/100		o,c
best.Alt	aircraft altitude from the GPS, if available; otherwise, barometric altitude; scaled by 1/1000		o,c
SkyCon	sky condition	clear, partly cloudy, overcast	o,c
♦*catIcePct*	percent sea ice cover	{<10%, ≥10%}	c
☺*Observer*	Observer Initials	{LB, RH}	o

*Turbo Commander univariate model did not converge.

**Group sizes in the Twin Otter did not range high enough for this covariate to be relevant.

♦Sea ice coverage during Twin Otter surveys was too sparse for this covariate to be relevant.

☺There were too many observers on the Turbo Commander surveys for this covariate to be meaningful.

Table 2. -- Summary statistics from August 2019 Bering-Chukchi-Beaufort Seas bowhead whale abundance survey and parameter estimates from the resulting abundance analysis. Bootstrap CVs presented here excluded iterations in which the abundance estimate for any single stratum was zero. CAPs = Cetacean Aggregation Protocols (Clarke et al. 2020).

Survey Region	**Amundsen Gulf**		**Eastern Beaufort Sea**		**Western Beaufort Sea**	**Total**
Aircraft	**Twin Otter**	**Turbo Commander**	**Twin Otter**	**Turbo Commander**	**Turbo Commander**	
number of bowhead whale sightings	1	1	57	88	12	**159**
number of bowhead whales	1	1	89	129	19	**239**
number of unidentified large cetacean sightings	0	0	2	2	1	**5**
number of unidentified large cetaceans	0	0	2	2	1	**5**
number of CAPs sessions	0	0	0	3	0	**3**
number of bowhead whale sightings on CAPs	0	0	0	20	0	**20**
transect and CAPs effort (km)	397.7	580.4	3,502.9	5,075.2	3,397.9	**12,954.1**
area surveyed (km^2)	1,577.6	3,340.4	15,520.9	28,730.4	19,445.4	**68,614.7**
*transect detection probability, $\hat{P}_0$	0.727					
*CV($\hat{P}_0$)	0.149					
availability bias correction factor, $\hat{P}_A$	0.159	0.198	0.177	0.208	0.207	
CV($\hat{P}_A$)	0.033	0.088	0.034	0.086	0.096	
**estimated abundance, $\hat{N}$	275		13,207		1,049	**14,531**
**CV($\hat{N}$)	0.550		0.570		0.538	**0.540**

*A single $\hat{P}_0$ was used for all aircraft and regions.

**Regional abundance estimates presented here represent both aircraft.

Table 3. -- Multiple covariates distance sampling detection function (g(y,z)) parameter estimates for the Twin Otter and Turbo Commander aircraft with observation-specific right-truncation distances. The hazard-rate key function was used for both models.

Twin Otter		
	Estimate	SE
Scale Coefficients		
Intercept	0.44	1.163
best.Alt	-1.088	0.913
Shape Coefficients		
Intercept	0.733	0.192

Turbo Commander		
	Estimate	SE
Scale Coefficients		
Intercept	-1.224	0.265
best.Alt	0.907	0.166
catIcePct1	-0.51	0.135
iBeauf	-0.047	0.031
Shape Coefficients		
Intercept	0.779	0.053

Table 4. -- Number of sightings, by species, in the ASAMM line-transect survey data and imagery data used to build the mark-recapture distance-sampling model to estimate transect detection probability, $\hat{P}_0$.

	ASAMM Line-transect Survey Data	**Imagery**
Bowhead whales	290	54
Gray whales	76	17
Humpback whales	20	1
Fin whales	4	0
Total	**390**	**72**

Table 5. -- Parameter estimates for the linear mixed models (Eqn. 5) of forward viewing distance for the left and right sides of the Turbo Commander. γ: Intercept. $\beta_{pdist.scl}$: Fixed effect of perpendicular sighting distance (scaled) on the slope. α_{obs}: Random effect of observer on the intercept. ε: Residual error.

	Left Side of Plane		**Right Side of Plane**	
	Estimate	**Standard Deviation**	**Estimate**	**Standard Deviation**
Fixed Effects				
γ	4430.2	442.2	4635.9	538.40
$\beta_{pdist.scl}$	221.8	117.6	297.52	92.68
Random Effects				
α_{obs}	--	1045.8	--	1299.9
ε	--	563.6	--	444.4

Table 6. -- Results of the bootstrap uncertainty estimation and sensitivity analyses. The number of bootstrap iterations used to estimate the associated CV is n_{iter}. n_{iter} may be less than 10,000 iterations due to lack of convergence in the multiple covariates distance sampling or mark-recapture distance sampling models, or because the bootstrap estimate of abundance for at least one stratum equaled zero.

Parameter	**n_{iter}**	**CV**
Total abundance	9004	0.540
Abundance in the Amundsen Gulf stratum	9004	0.550
Abundance in the eastern Beaufort Sea stratum	9004	0.570
Abundance in the western Beaufort Sea stratum	9004	0.538
Total abundance, fixing p0 at point estimate	9004	0.387
Total abundance, fixing weighted p(availability) for the Commander at point estimate	9004	0.548
Total abundance, fixing p(availability) for the Otter at point estimate	9004	0.540
Total abundance, fixing ASAMM survey effort and sighting data	10000	0.322
p0	10000	0.149
Otter time-in-view	10000	0.127
Commander (right side of plane) time-in-view	10000	0.342
Commander (left side of plane) time-in-view	10000	0.281
Commander Amundsen Gulf weighted p(availability)o	6895	0.088
Commander eastern Beaufort Sea weighted p(availability)	10000	0.086
Commander eastern Beaufort Sea weighted p(availability)	10000	0.086
Commander western Beaufort Sea weighted p(availability)	9998	0.096
Otter Amundsen Gulf weighted p(availability)	6856	0.033
Otter eastern Beaufort Sea weighted p(availability)	10000	0.034

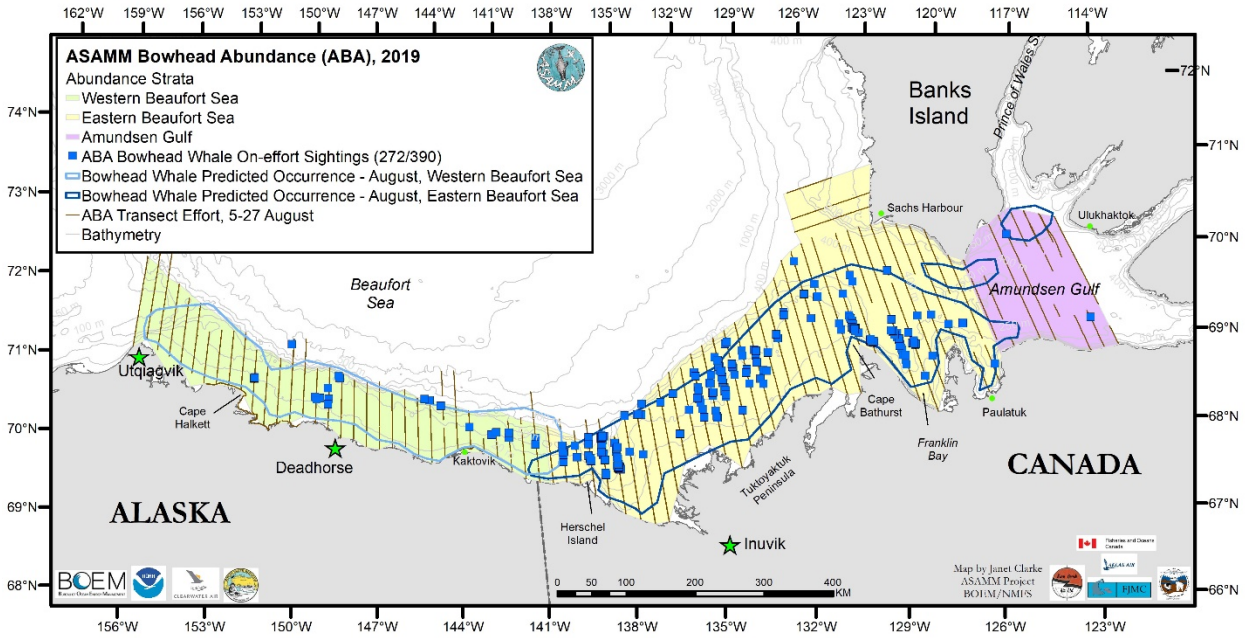

Figure 1. -- Study area and regions (strata) for the Aerial Surveys of Arctic Marine Mammals (ASAMM) bowhead abundance survey in 2019. The polygons outlined in light and dark blue indicate the expected distribution of bowhead whales in the study area during August based on all available information, including Indigenous knowledge, historical whaling records, previous aerial surveys, and telemetry studies. Survey effort and bowhead whale sightings (number of sightings/number of whales) from the August 2019 survey period are also shown. The primary bases of operations were Inuvik, Northwest Territories, Canada, and Deadhorse, Alaska, USA.

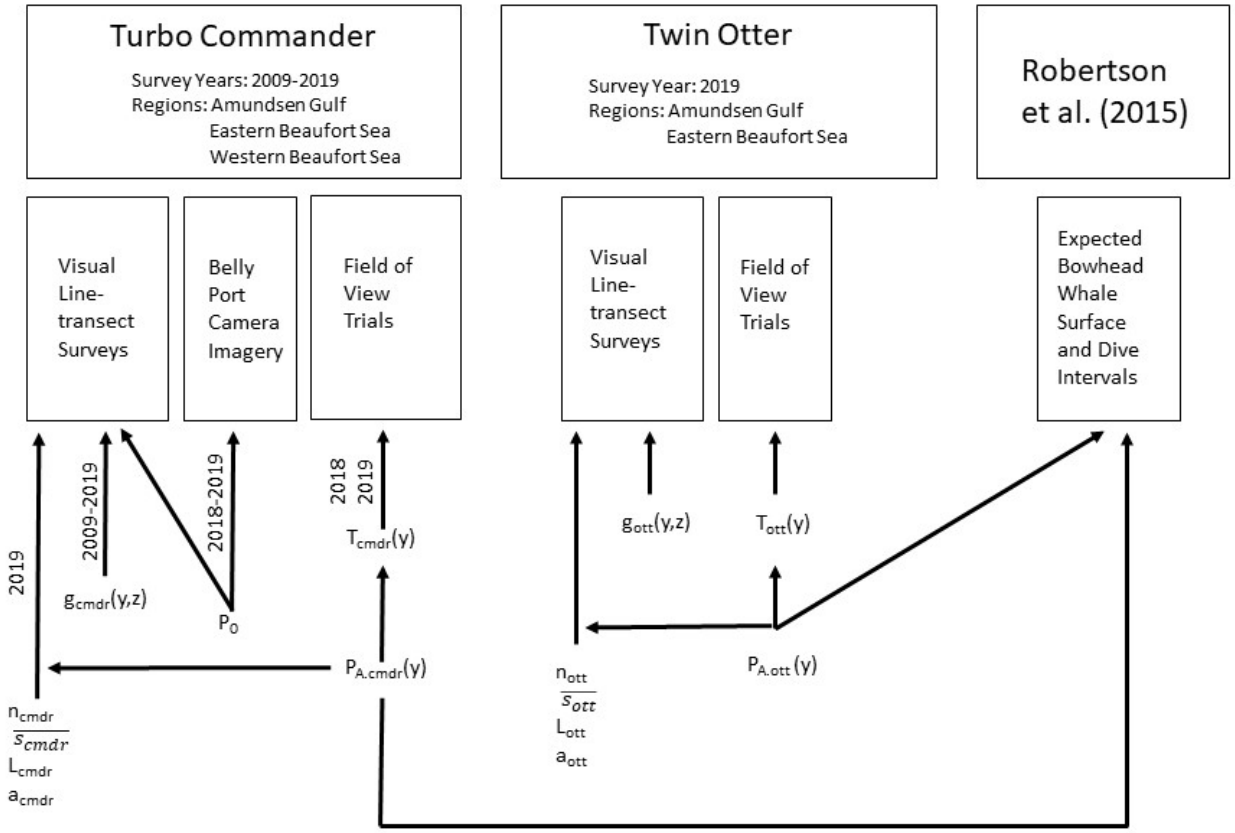

Figure 2. -- Data sources and subsets used to estimate parameters for the Bering-Chukchi-Beaufort Seas bowhead whale abundance estimate. cmdr = Turbo Commander. ott = Twin Otter. See text for definitions of variables and parameters.

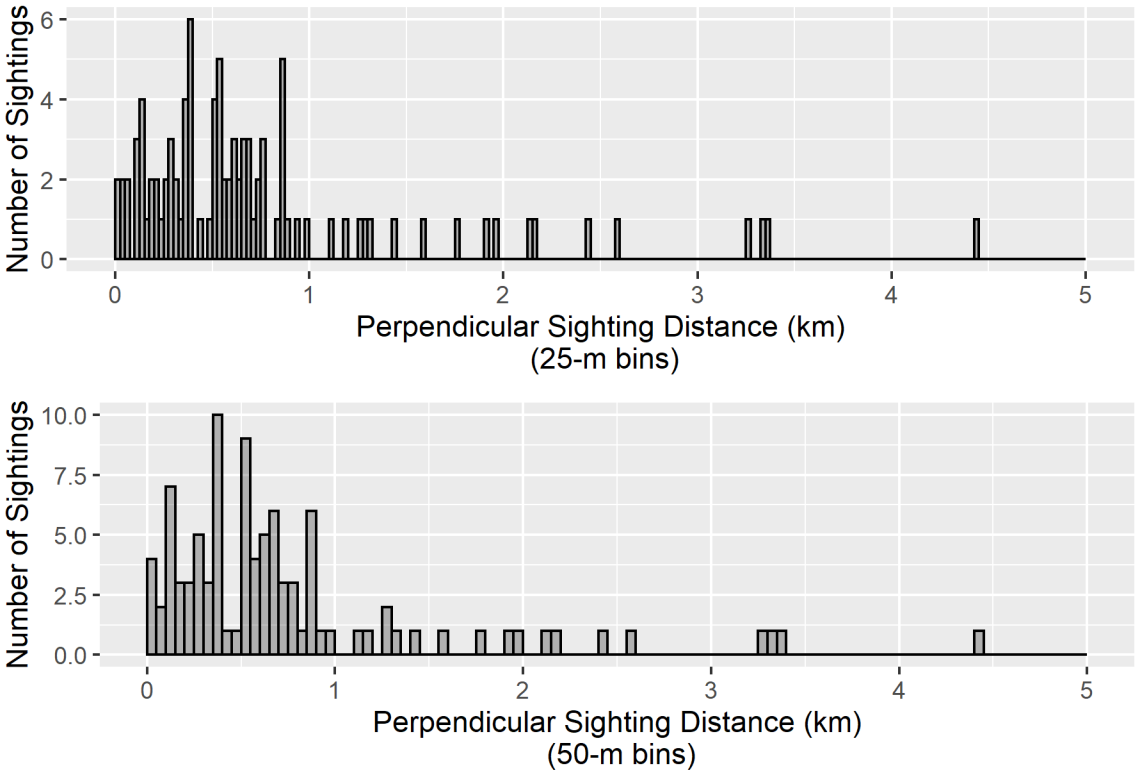

Figure 3. -- Histograms of perpendicular distance to bowhead whale sightings by primary observers on the Twin Otter aircraft during the August 2019 line-transect surveys. To examine the effect of bin size on the distribution of perpendicular distances, the histogram in the top figure uses 25-m bins and the bottom figure uses 50-m bins.

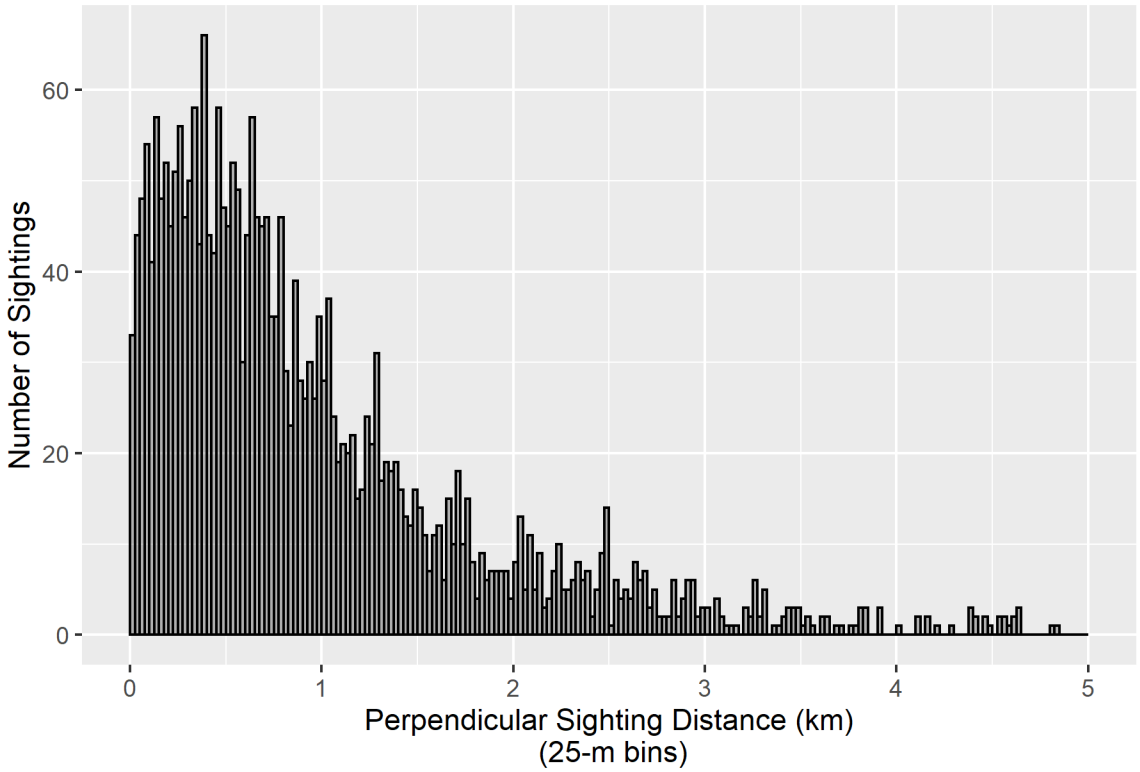

Figure 4. -- Histogram of perpendicular distances to bowhead whale sightings by primary observers on the Turbo Commander aircraft during ASAMM line-transect surveys from 2009 to 2019. This histogram uses 25-m bins.

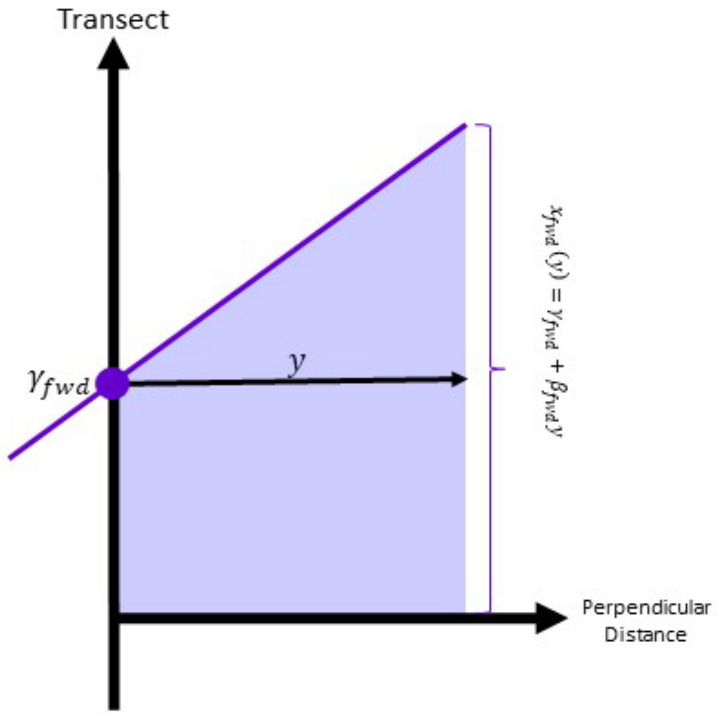

Figure 5. -- Schematic representation of a simple linear model for estimating parameters defining the forward (fwd) field of view for the primary observer on the right side of the aircraft. x is the viewing distance. γ is the intercept. β is the slope. y is the perpendicular distance to the transect.

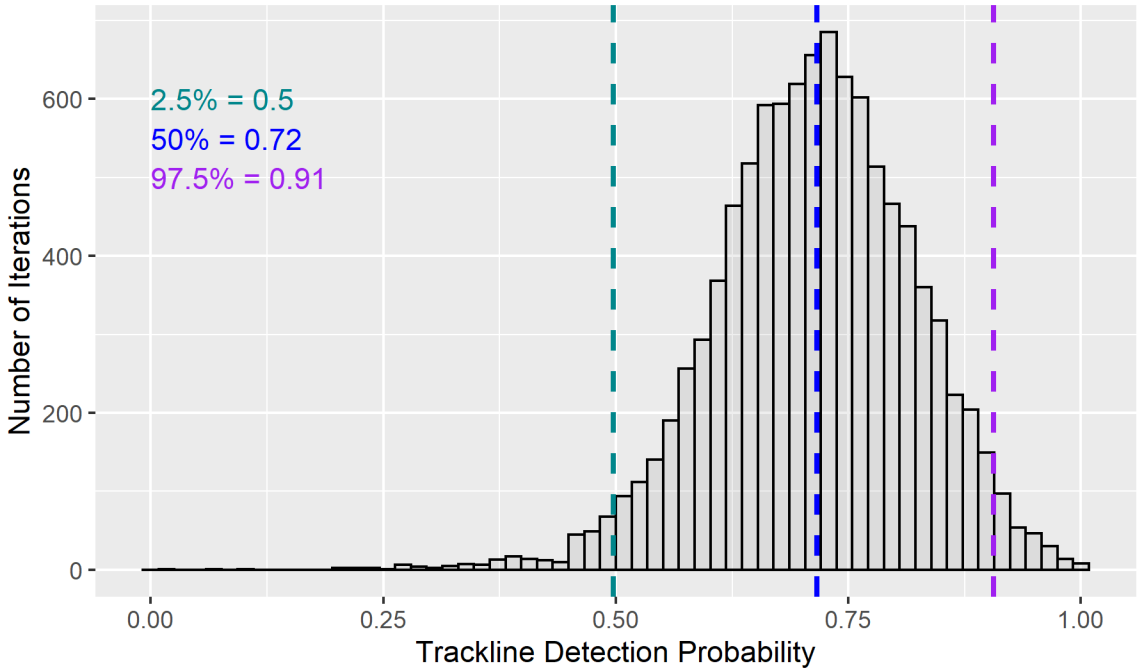

Figure 6. -- Sampling distribution for transect detection probability, $\hat{P}_0$, generated using the bootstrap algorithm (Appendix). The 2.5%, 50%, and 97.5% quantiles are shown as dashed vertical lines.

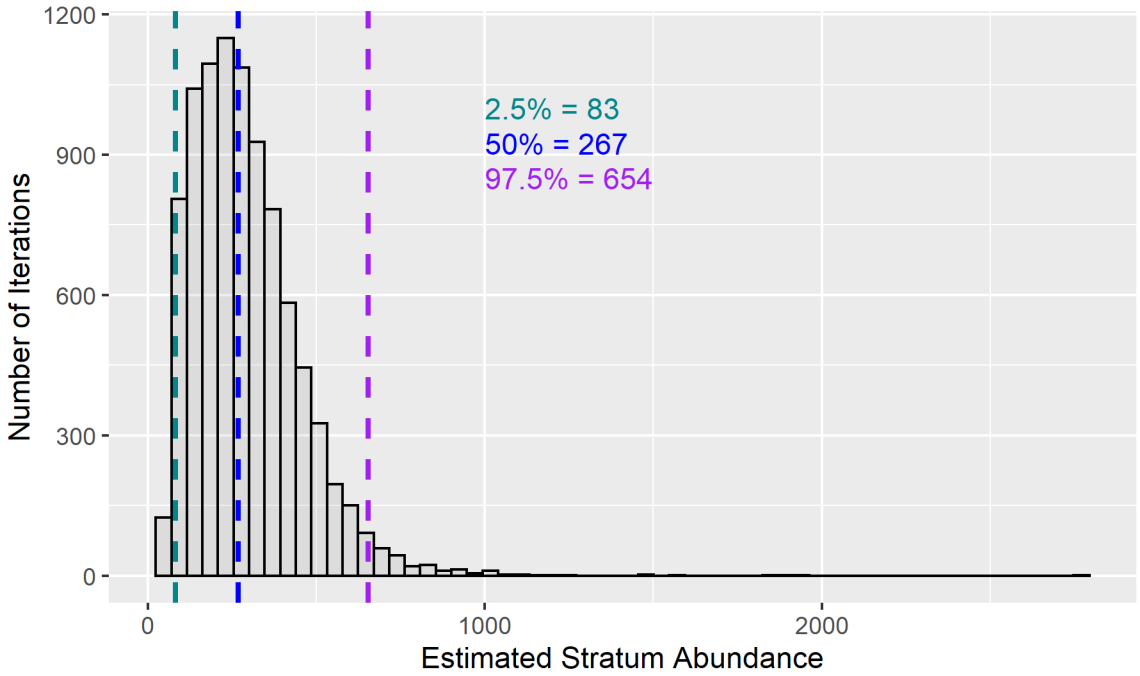

Figure 7. -- Sampling distribution for BCB bowhead whale abundance in the Amundsen Gulf region, generated using the bootstrap algorithm (Appendix). The 2.5%, 50%, and 97.5% quantiles are shown as vertical lines.

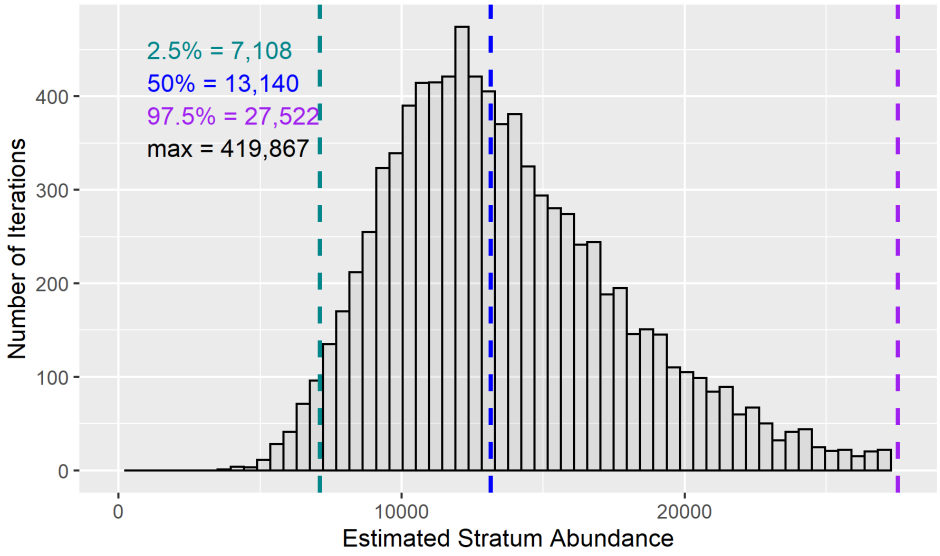

Figure 8. -- Sampling distribution for BCB bowhead whale abundance in the eastern Beaufort Sea region, generated using the bootstrap algorithm (Appendix). The 2.5%, 50%, and 97.5% quantiles are shown as vertical lines. The distribution was truncated at the 97.5% quantile. The maximum bootstrap estimate of abundance for the region was 419,867 whales.

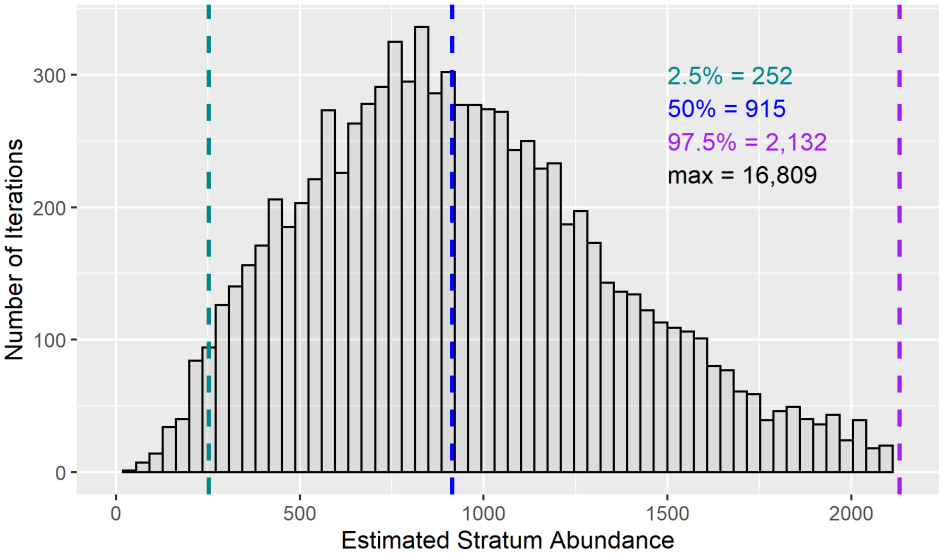

Figure 9. -- Sampling distribution for BCB bowhead whale abundance in the western Beaufort Sea region, generated using the bootstrap algorithm (Appendix). The 2.5%, 50%, and 97.5% quantiles are shown as vertical lines. The distribution was truncated at the 97.5% quantile. The maximum bootstrap estimate of abundance for the region was 16,809 whales.

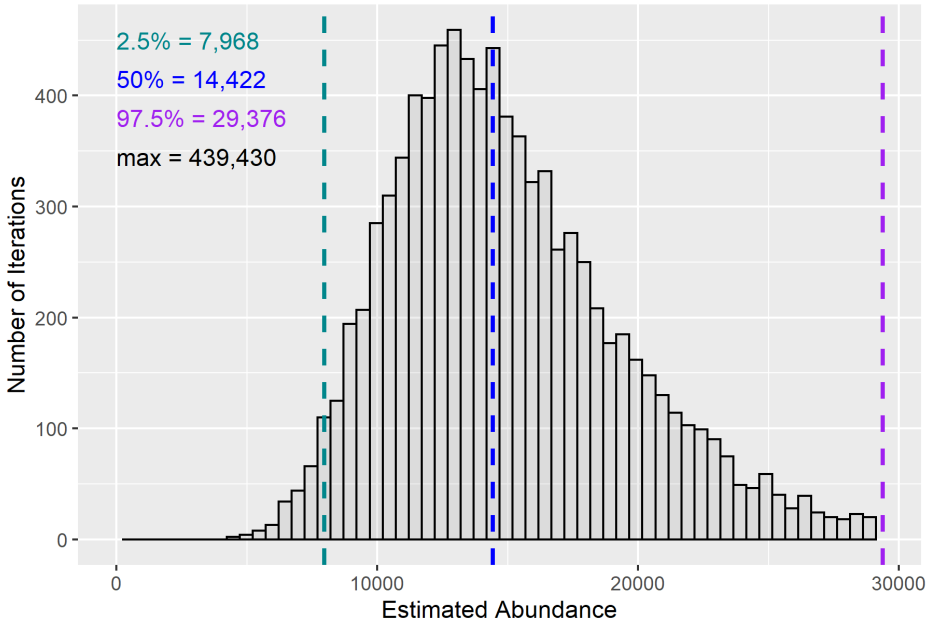

Figure 10. -- Sampling distribution for BCB bowhead whale abundance in the overall August 2019 aerial line-transect survey study area, generated using the bootstrap algorithm (Appendix). The 2.5%, 50%, and 97.5% quantiles are shown as vertical lines. The distribution was truncated at the 97.5% quantile. The maximum bootstrap estimate of total abundance was 439,430 whales.

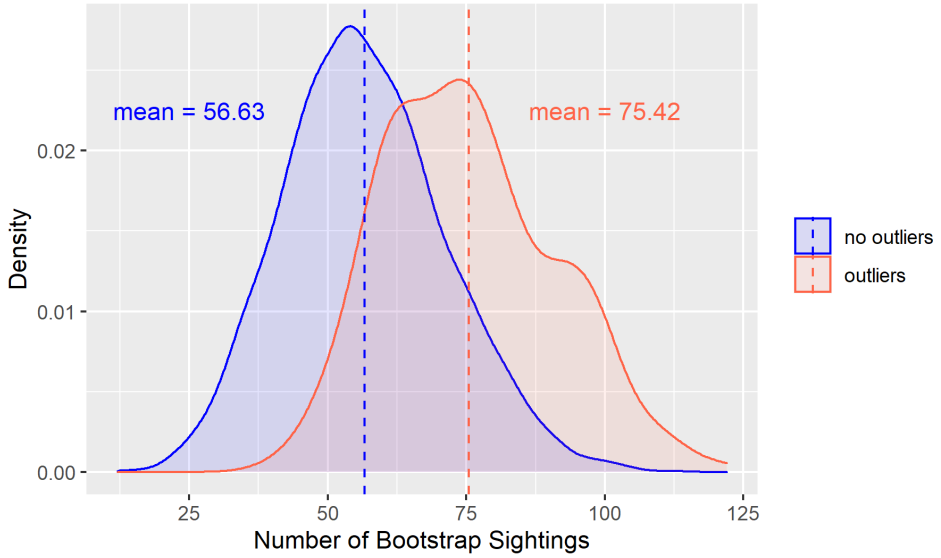

Figure 11. -- Sampling distribution for the number of bootstrap sightings of bowhead whales in the eastern Beaufort Sea region for two subsets of bootstrap iterations: iterations resulting in bootstrap estimates of total abundance that were outliers (Eqn. 9) and those that did not result in outliers. The mean number of bootstrap sightings was 75.42 in the subset of iterations with outliers and 56.63 in the subset of iterations without outliers.

Appendix

Pseudocode for the bootstrap algorithm to estimate uncertainty in the 2019 BCB bowhead whale abundance estimate from aerial line-transect surveys

This pseudocode generates bootstrap samples to estimate uncertainty in the following parameter estimates:

- $T^{aircraft}\left(y_{ltrnc}^{aircraft}\right)$: time-in-view at the left-truncation distance y_{ltrnc} for the Turbo Commander (aircraft = "c") and Twin Otter (aircraft = "o");
- P_0 : trackline detection probability;
- $P_{A,aircraft,reg}$: availability bias correction factor, defined as the probability that a bowhead whale in region "reg" is available to be seen by an aerial visual observer at the aircraft's left-truncation distance. Regions correspond to "AG" for Amundsen Gulf, "EBS" for the eastern Beaufort Sea, and "WBS" for the western Beaufort Sea. This parameter is derived separately for each region and aircraft as a weighted average of the availability bias correction factors for bowhead whales in five different activity states, with weights corresponding to the proportion of bowhead whale sightings engaged in each activity state;
- $P_{i,aircraft}$: average detection probability for an aerial visual observer, assuming P_0=1.0, for the Turbo Commander and Twin Otter aircraft; and
- N_{reg}: bowhead whale abundance by survey region.

Sample units have unique sample labels. Sample units and sample labels are specified by the combination of aircraft type, survey year, and transect number.

for b in 1:nboot{

Each bootstrap sample and parameter estimate technically should have a subscript "b" indicating the bootstrap iteration number. For simplicity, the "b" subscripts have been omitted from the text below.

I. Generate a parametric bootstrap sample of time-in-view at the left-truncation distance y_{ltrnc}^{c} for the Turbo Commander, $T^{c}(y_{ltrnc}^{c})$.
   1. Simulate n_R and n_L samples from the original FOV models for the right side of plane (SOP) and the left SOP, respectively. n_R and n_L represent the sample sizes used to create the original FOV models for the right and left SOP.
   2. Refit the FOV models for the right and left SOP with the simulated data.
   3. Use the new FOV models to predict viewing distances $x_{ltrnc,R}^{c}$ and $x_{ltrnc,L}^{c}$ at perpendicular distance y_{ltrnc}^{c} for a "new" observer.
   4. Convert $x_{ltrnc,R}^{c}$ and $x_{ltrnc,L}^{c}$ to time-in-view by dividing by the aircraft's survey speed: $T_{sop}^{c}(y_{ltrnc}^{c}) = x_{ltrnc,sop}^{c}/speed$.
   5. Let the time-in-view value for bootstrap iteration b equal the average of $T_R^c(y_{ltrnc}^{c})$ and $T_L^c(y_{ltrnc}^{c})$: $T^{c}(y_{ltrnc}^{c}) = \frac{T_R^c(y_{ltrnc}^{c})+T_L^c(y_{ltrnc}^{c})}{2}$.

II. Generate a parametric bootstrap sample of time-in-view at the left-truncation distance for the Twin Otter, $T^{o}(y_{ltrnc}^{o})$.
   1. Simulate n samples from the original FOV model for the Twin Otter, where n represents the sample size used to create the original FOV model.
   2. Refit the FOV model for the Twin Otter with the simulated data.
   3. Use the new FOV model to predict viewing distance x_{ltrnc}^{o} at perpendicular distance y_{ltrnc}^{o}.
   4. Convert x_{ltrnc}^{o} to time-in-view by dividing by the aircraft's survey speed: $T^{o}(y_{ltrnc}^{o}) = x_{ltrnc,sop}^{o}/speed$.

III. Generate a non-parametric bootstrap sample of trackline detection probability, P_0.
   1. Determine the number of unique sample labels represented by the imagery sightings of large whales. Call this number n_{unq}. This step needs to be completed only once, and can be done prior to running the bootstrap algorithm.
   2. Resample n_{unq} sample labels with replacement from the original set of unique sample labels represented by the imagery sightings of large whales.
   3. Extract the ASAMM observer and imagery sightings associated with the bootstrap set of sample labels. Sample labels that were drawn multiple times will enter into the bootstrap dataset multiple times.
   4. Refit the mrds model using the bootstrap dataset of observer and imagery sightings.
   5. Save the predicted value of P_0 and sample size information: total number of observations, observations by observer 1, observations by observer 2, and duplicate observations.

IV. For the Turbo Commander, generate non-parametric bootstrap samples of line-transect sightings and effort, refit the mcds model, and recalculate the region-specific availability bias correction factors, $P_{A,c,reg}$
   1. Determine the number (n_{reg}) and identity of unique sample labels in each region (reg = AG, EBS, or WBS), in the August 2019 line-transect survey dataset. Some sample labels will correspond to sample units without bowhead whale sightings. This step needs to be completed only once, and can be done prior to running the bootstrap algorithm.
   2. For each region, draw n_{reg} sample labels, with replacement, from the original set of unique sample labels for that region in August 2019. Extract the corresponding information on survey effort (km), area covered ($a_{e,c,reg}$, km^2), and sightings by sample unit. Each draw represents a unique bootstrap sample.
   3. Determine the number (n_c) and identity of unique sample labels with bowhead whale sightings on transect, search, or CAPs passing in the 2009-2019 Turbo Commander line-transect survey dataset. This step needs to be completed only once, and can be done prior to running the bootstrap algorithm.
   4. Draw n_{new} additional sample labels from the 2009-2019 dataset referenced in step IV.3. n_{new} represents the number of additional bootstrap samples needed to bring the total number draws for this bootstrap iteration to n_c. Extract the sighting data corresponding to the sample units. Each draw represents a unique bootstrap sample.
   5. Refit the Turbo Commander mcds model using the full set of samples for this bootstrap iteration. Predict $P_{i,c}$ for each sighting in the bootstrap samples drawn in step IV.3. $P_{i,c}$ is the average detection probability, assuming P_0=1.0, given the observation-specific right-truncation distance w_i:
$$P_{i,c} = \frac{1}{w_i}\int_{ltrnc}^{w_i} g(y,z)dy.$$
   6. Recompute $P_{A,c,reg}$ for each region based on $T^c(y^c_{ltrnc})$ generated in step I, the mean surface and dive durations from Robertson et al. (2015), and the proportion of bootstrapped bowhead whale sightings engaged in each activity type in each region. Save the regional estimates of $P_{A,c,reg}$.

V. Repeat step IV using the Twin Otter line-transect survey data and $T^o(y^o_{ltrnc})$ generated in step II.

VI. Compute and save the bootstrap abundance estimates for each region, N_{reg}, using the bootstrap samples for sightings, P_0, $P_{A,aircraft,reg}$, $P_{i,aircraft}$, and $a_{e,aircraft,reg}$.

}

November 2021

www.nmfs.noaa.gov

OFFICIAL BUSINESS

National Marine Fisheries Service
Alaska Fisheries Science Center
7600 Sand Point Way N.E.
Seattle, WA 98115-6349